years (range, 22–78), and median Karnofsky Performance Scale (KPS) was 70 (30–80) (Table 1). Five patients underwent RT plus concomitant TMZ at the initial therapy, and others received TMZ monotherapy on disease progression. BV treatment was primarily (67 %) given as the second line therapy (range 2–5). The cycles of BV therapy ranged from 1 to 21 (median 7). There were no serious adverse events in any of the patients.

Response to BV

After the first BV cycle, early post-treatment MR imaging (taken between days 3 and 21, median 13) demonstrated rapid shrinkage of both enhancing and T2-elongated (hyperintense on T2-weighted and FLAIR images) areas in most tumors (Fig. 1). By a patient-based analysis, single BV treatment resulted in a decrease in evaluable enhancing tumor volume in eight of nine cases (88.9 %) (Table 1). Four patients (44.4 %) had a partial response (PR), four had a stable disease (SD), and one had a progressive disease (PD) by the Macdonald criteria; the overall response rate was 44.4 %. In cases 1, 3, and 8, both hemiparesis and disturbance of consciousness recovered soon after the first BV administration with a marked reduction of extent of hyperintensity on T2-weighted or FLAIR images along with the enhancing tumor shrinkage. KPS improved immediately in four cases (44.4 %).

Association of tumor mADC values with the response to BV

Of 15 individual evaluable enhancing lesions in the nine patients, 11 tumors shrank (Fig. 1), while four did not respond upon initial BV treatment (Fig. 2). We then evaluated parameters obtained in the MR images to determine if there were any predictors for tumor response to BV. The pretreatment MR images were obtained on days −1 to −25 (median −10). The average pretreatment mADC value for all lesions was 1249 (10^{-6} mm^2/s) (range 964–1672). Tumor mADC values were above 1100 in all of the responding tumors, in contrast to those in all non-responding lesions that scored below 1100 (Fisher's exact test, $p = 0.001$) (Fig. 3), suggesting that a pretreatment mADC value higher than 1100 may be predictive for a rapid shrinkage of enhancing tumors. Interestingly, the tumor mADC values decreased significantly after the first BV treatment in all lesions except for one that did not respond (paired t test, $p < 0.001$) (Fig. 4). The average mADC value after the first cycle of BV was 1051 (range 828–1320).

To determine whether the mADC value after the first BV treatment (post-BV mADC) could also predict a further response of the lesion to additional cycles of BV, the ratio

Table 1 Summary of cases treated with bevacizumab monotherapy on temozolomide failure

No	Age (years)	Gender	KPS (pre-BV)	Pathological Dx	RT (Gy)	TMZ cycles	TMZ OR	*MGMT* status	BV line[a]	BV cycles	Months from last RT	mADC (pre-BV) (10^{-6} mm^2/s)	Total TV (ml) (pre-BV)	BV OR	Relative TV[b]	KPS (post 1st BV)	Relapse	PFS (months)	Out-come	OS (months)
1	74	Female	40	AA	60	46	CR	nd	3	7	77	1394	61.7	SD	0.63	50	+	2.2	D	5.7
2	51	Male	70	AA	60 + SRT	14	SD	nd	2	21	15.2	1354	45.0	PR	0.03	70	+	7.7	D	16.0
3	60	Female	70	GBM	60 + SRT	11	SD	M	2	4	5.6	964–1490[c]	25.7	SD	0.88	90	+	1.5	D	3.3
4	32	Female	70	GBM-s	50	10	SD	M	3	8	35.8	1190	23.7	SD	0.73	70	+	2.3	D	5.5
5	22	Male	80	GBM-s	60	1	PD	U	2	12	2.1	1273	16.8	PR	0.13	80	+	5.5	D	10.3
6	73	Female	60	GBM	60	5	SD	U	2	1	6.7	1009–1281[c]	7.9	PD	1.78	50	+	0.4	D	3.9
7	58	Female	80	GBM	60	8	SD	U	2	8	7.6	1323	8.4	PR	0.67	80	+	3.9	D	11.1
8	51	Female	30	GBM	60 + SRT	40	CR	M	5[a]	5	4.3	1281	152.8	SD	0.54	50	+	1.4	D	2.9
9	78	Male	30	GBM	40	1	PD	U	2	3	1.9	1257–1672[c]	72.9	PR	0.24	40	+	2.1	D	8.3

KPS Karnofsky Performance Scale, *Dx* diagnosis, *RT* radiotherapy, *TMZ* temozolomide, *OR* objective response, *MGMT* O^6-methylguanine-DNA methyltransferase, *BV* bevacizumab, *mADC* mean apparent diffusion coefficient, *pre-BV* before the first BV treatment, *TV* tumor volume, *PFS* progression-free survival, *OS* overall survival, *AA* anaplastic astrocytoma, *GBM* glioblastoma, *GBM-s*, secondary GBM, *SRT* stereotactic radiotherapy, *CR* complete response, *PR* partial response, *SD* stable disease, *PD* progressive disease, *nd* not determined, *M* methylated promoter, *U* unmethylated promoter, *D*, dead

[a] Previous chemotherapy included bevacizumab

[b] The ratio of tumor volume at the first MR imaging post-bevacizumab treatment compared with that of the baseline

[c] The lowest and highest values of multiple lesions

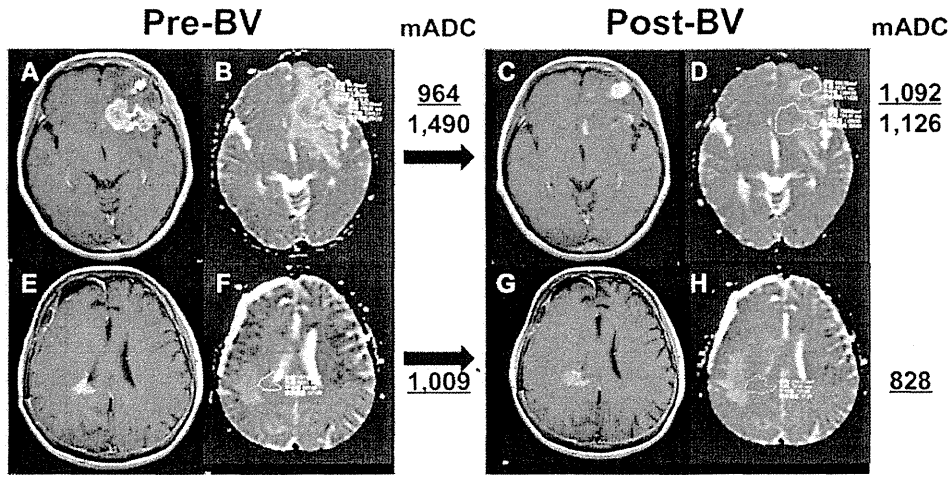

Fig. 2 Post-contrast T1-weighted images aligned side-by-side with the corresponding ADC maps in patients with tumors which did not respond to BV (**a, b, c, d**: case 3; **e, f, g, h**: case 6). Note that the non-responding lesions have mADC values below 1100 (10^{-6} mm^2/s). In case 3, the anterior frontal lesion with an initial mADC of 964 continues to grow, whereas the posterior frontal lesion that has undergone stereotactic radiotherapy before further progression shows an initial mADC of 1490 and its enhancement reduces after BV treatment

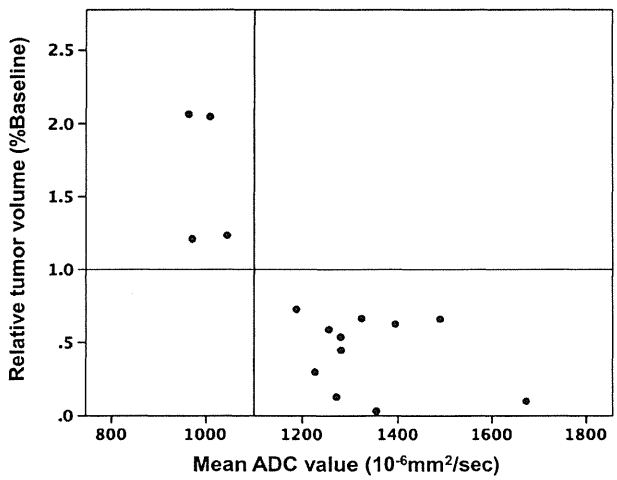

Fig. 3 Clear correlation between mean ADC values and changes in tumor size after a single BV treatment in recurrent high-grade glioma lesions. All lesions with mADC above 1100 (10^{-6} mm^2/s) shrink, while those with lower mADC continue growth (Fisher's exact test, $p = 0.001$)

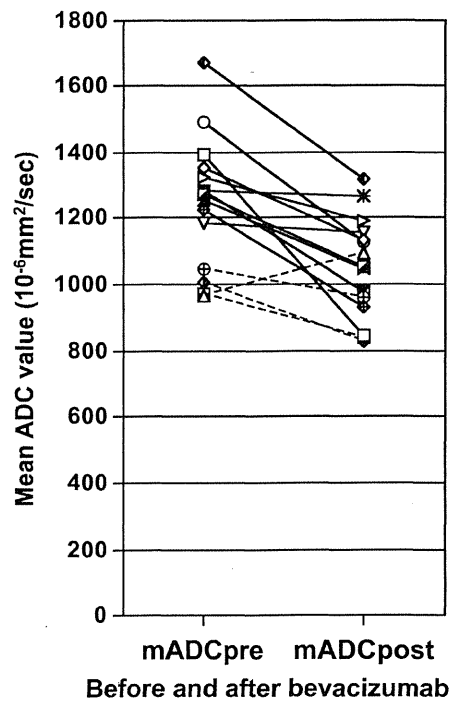

Fig. 4 Changes in mADC value between pre- and post-treatment with BV. Corresponding mADC value points of each lesion are connected with *lines*; the responding lesions are in *solid lines* and the non-responding are in *dashed lines*. mADC values of all lesions decrease after BV except for one non-responding

of tumor volumes at the first MR imaging to those at the second MR imaging taken after 2 more BV cycles (median interval, 39 days; range, 35–56 days) was measured (Table 2). Post-BV mADC significantly correlated with response to additional BV (Mann–Whitney U test, $p = 0.045$) and all five high post-BV mADC (>1100) lesions shrank after the additional BV treatments. Although three of eight (37.5 %) low post-BV mADC (<1100) lesions also decreased in size, the majority (5/8, 62.5 %) did not respond further, which approached statistical significance (Fisher's exact test; $p = 0.075$). These observations suggest that even the mADC immediately after the first BV treatment may be of predictive value for further response to BV.

Table 2 mADC values before and after the first bevacizumab treatment and the change in tumor volume

Case	Lesion	mADC (10^{-6} mm^2/s)		TV (%baseline) (1st F/U MRI)	TV (%baseline) (2nd F/U MRI)	TV (%1st MRI) (2nd F/U MRI)
		Before	After			
1	P/T	1394.2	842.5	62.7	21.8	34.9
2	T	1353.6	1135.8	3.3	0.0	0.0
3	F	1490.1	1125.6	66.1	63.6	96.3
	F-AL	964.3	1092.0	206.4	445.5	215.9
	F-AM	971.1	841.1	120.9	135.5	112.1
	F-MF	1227.6	930.0	29.8	30.4	103.1
	F-PM	1044.5	961.8	123.2	225.6	183.1
4	F-BG	1187.5	1155.4	72.8	15.2	20.9
5	T	1272.6	1053.0	12.9	0.0	0.0
6	T	1008.9	827.6	204.6	na	na
	F	1281.1	1267.7	44.8	na	na
7	CC	1323.4	1192.9	66.5	18.3	27.9
8	PT	1280.9	977.4	53.8	106.7	198.4
9	F	1672.4	1320.5	10.0	7.3	73.7
	F	1256.7	1046.5	58.9	50.1	85.1

TV, tumor volume, *F/U* follow-up, *P* parietal, *T* temporal, *F* frontal, *AL* antero-lateral, *AM* antero-medial, *MF* mid-frontal, *PM* premotor, *BG* basal ganglia, *CC* corpus callosum

Survival

After a median follow-up of 5.7 months (range, 2.9–16.0), all patients had progressed and died despite a high rate of early response. PFS from the initiation of BV therapy was 2.2 months [95 % confident interval (CI) 1.8–2.6 months]. PFS for two patients (cases 3 and 6) having a lesion with mADC value <1100 (low mADC) was short (0.4 months), whereas PFS for others having all lesions with mADC >1100 (high mADC) was significantly longer (2.3 months, 95 % CI 2.0–2.6) (log-rank test, $p = 0.018$). Median OS after the start of BV treatment was 5.7 months (95 % CI 5.1–6.2). Patients having all lesions with a high mADC (>1100) survived significantly longer (median 8.3 months, 95 % CI 1.4–15.2) than those with a low mADC tumor(s) (median 3.3 months, $p = 0.046$), despite the small sample number (9 cases). The tumor volume of enhancing lesions prior to initiation of BV was not associated with either PFS or OS (Table 1, data not shown).

VEGF expression in the original tumor specimens

Immunohistochemistry staining of VEGF-A was performed in the primary tumors and all but one were found to express VEGF to a variable extent (data not shown). Expression at the beginning of BV treatment was not determined due to lack of re-resection prior to BV therapy. The tumor with negative VEGF staining (case 6) did not respond to BV.

Relationship of mADC with *MGMT* promoter methylation status

While *MGMT* status is prognostic/predictive for survival in GBM patients [17, 18], tumoral mADC values were not associated with *MGMT* methylation status (Fisher's exact test; $p = 0.445$) in the seven GBM cases (Table 1). Taken together, while we observed that response of recurrent lesions after a single dose of BV was significantly correlated with a mean ADC value of the tumors above 1100 (10^{-6}mm^2/s), it was not with VEGF expression or *MGMT* status.

Discussion

Although BV has shown efficacy against TMZ-refractory GBMs, some tumors may also be resistant to BV, progressing to fatality [19], and thus determining their sensitivity to BV prior to initiation of the treatment could have significant clinical value. Here, we demonstrated that the pretreatment mADC value of enhancing tumors was predictive for initial response to BV monotherapy in recurrent HGGs. All lesions with the mADC above 1100 (10^{-6} mm^2/s) responded, in clear contrast to those with the mADC below 1100, which did not respond ($p = 0.001$) (Fig. 3). The mADC values decreased after the first BV treatment in all lesions, except for one that did not respond. The second mADC value obtained after the first BV treatment was also a good indicator for further response to additional BV when it remained above 1100 ($p = 0.045$). Furthermore, the high mADC value also significantly correlated with elongation of both PFS and OS after BV treatment in patients with TMZ-refractory recurrent HGGs.

Anti-VEGF therapy is expected to normalize vascular structure, capillary permeability and interstitial pressure more effectively in areas with strong edema and necrotic changes than in those with "packed" tumor cells. The ADC value represents movement of protons of water molecules and may be increased in areas where tissue edema and necrotic components have been induced by tissue damage from tumor burden and cytotoxic therapies [9–11]. This may account for our findings that glioma lesions with a high pretreatment ADC value shrank upon BV challenge whereas those with a low ADC value did not. Such non-responding lesions also tended to be strongly enhanced (e.g., a subcortical lesion in the left frontal lobe in Fig. 2a), consistent with the observation that GBMs that relapsed after BV treatment exhibited low ADC values and hyperintensity on diffusion-weighted images [20].

Pope et al. reported that PFS correlated with crude average ADC values within areas showing contrast enhancement in 41 recurrent GBM cases who underwent BV treatment. Of note, when the average ADC value of the lower peak of biphasic peaks in ADC histograms ($mADC_L$) was lower than 1201, PFS was significantly extended [21]. Our use of whole ADC values within an enhancing tumor to calculate a mean value on a PACS terminal in clinics without specific software successfully segregated responding from non-responding lesions. This simple method might incorporate regions of extremely high ADC values containing necrotic tissues, resulting in a shift of the mean value toward a higher value, compared with the histogram-based analysis. However, regions exhibiting apparent necrosis or cyst could be readily excluded when defining a tumor on each ADC map, in order to avoid such data contamination. We also eliminated T2-elongated areas surrounding contrast-enhancing lesions because they may contain both edematous white matter and non-enhancing tumor to a variable extent. As a result, our data show clear segregation of lesions for response by ADC value at 1100 (10^{-6} mm^2/s), smaller than the cut-off value of 1201 in the Pope study [21]. It would be beneficial in daily practice to use this simple measurement, as it does not require specific histogram analysis, though it needs further accumulation of cases for validation.

Conflicting findings that BV induces rapid shrinkage of the enhancing lesions while they subsequently regrow in a relatively short term might represent, at least partly, the recently recognized "pseudo-response," a decrease in enhancing tumor on MR imaging without a decrease in tumor activity [22]. This has been reported in a clinical trial where radiation necrosis was successfully treated with BV [23]. To date, there are no validated imaging methods to determine whether the observed shrinkage of areas of contrast enhancement were due to real tumor reduction or pseudo-response, as well as progression without an emergence or increase of enhancing lesion [24]. Indeed, the potential value of changes in T2 relaxation time is recently suggested by an observation that an elevated residual, post-treatment, median T2 may be predictive of both PFS and OS [25]. Efforts to clarify these issues include application of the newly-developed response criteria, Response Assessment in Neuro-Oncology (RANO), utilizing elongation of T2 relaxation time as a surrogate for non-enhancing tumor [26], and MR imaging techniques such as MR perfusion studies that are under investigation in large trials for validity. In our study, there were two patients (cases 3 and 8) who underwent stereotactic RT on recurrence prior to BV initiation, and one patient (case 5) who received BV within 3 months after completion of induction-concomitant RT plus TMZ. Two of these three patients had a PR by single BV treatment with further progression in 2 and 5.5 months, indicating no clear relationship between response and potential radiation injury.

A recent study reported that the lower ADC_L value rather correlated with longer PFS for patients with newly-diagnosed GBM [27], in contrast to recurrent GBM. It also showed an association between ADC values and *MGMT* methylation status [27], which was not observed in our series. Whether this association might be influenced by the difference of tumor microstructure in the setting of newly-diagnosed or treatment-modified recurrent tumors needs to be clarified.

Limitations of our study include the small number of patients and lesions analyzed, heterogeneous prior treatment regimens applied in some patients, and specimens from primary newly-diagnosed tumors used for determination of VEGF and *MGMT* status. This might hamper drawing definite conclusions about the relationship of the mADC value with survival gain or VEGF/*MGMT* status, as well as analyzing whether pathological findings of treated tumors may also correlate with either mADC values or responsiveness to BV, or both. However, even with the small sample size, a clear segregation of responders from non-responders and survival prediction were seen using our simplified mADC measurement and this warrants further investigation in a larger series.

Conclusions

Bevacizumab monotherapy is an active regimen for patients with TMZ-refractory recurrent gliomas leading to rapid lesion shrinkage, and the tumor mADC value can be a useful marker for prediction of BV response and survival, and thus for patient selection. It would be also intriguing to investigate methods of delineating tumors in which BV would provide long-term response in the future.

Acknowledgments This work was supported partially by grants of the Ministry of Health, Labour, and Welfare of Japan (H20-ganrinsyou-ippan-019 and 20shi-4) (to MN). We thank Kuninori Kobayashi, RT (Radiology Section, Kyorin University Hospital) for obtaining MR imaging data.

Conflict of interest The authors declare that they have no conflict of interest.

References

1. Stupp R, Mason WP, van den Bent MJ et al (2005) Radiotherapy plus concomitant and adjuvant temozolomide for glioblastoma. N Engl J Med 352:987–996
2. Norden AD, Drappatz J, Wen PY (2009) Antiangiogenic therapies for high-grade glioma. Nat Rev Neurol 5:610–620

3. Fischer I, Gagner JP, Law M et al (2005) Angiogenesis in gliomas: biology and molecular pathophysiology. Brain Pathol 15:297–310
4. Yuan F, Chen Y, Dellian M et al (1996) Time-dependent vascular regression and permeability changes in established human tumor xenografts induced by an anti-vascular endothelial growth factor/vascular permeability factor antibody. Proc Natl Acad Sci USA 93:14765–14770
5. Chamberlain MC (2010) Emerging clinical principles on the use of bevacizumab for the treatment of malignant gliomas. Cancer 116:3988–3999
6. Vredenburgh JJ, Desjardins A, Herndon JE 2nd et al (2007) Bevacizumab plus irinotecan in recurrent glioblastoma multiforme. J Clin Oncol 25:4722–4729
7. Friedman HS, Prados MD, Wen PY et al (2009) Bevacizumab alone and in combination with irinotecan in recurrent glioblastoma. J Clin Oncol 27:4733–4740
8. Kreisl TN, Kim L, Moore K et al (2009) Phase II trial of single-agent bevacizumab followed by bevacizumab plus irinotecan at tumor progression in recurrent glioblastoma. J Clin Oncol 27:740–745
9. Sugahara T, Korogi Y, Kochi M et al (1999) Usefulness of diffusion-weighted MRI with echo-planar technique in the evaluation of cellularity in gliomas. J Magn Reson Imaging 9:53–60
10. Mardor Y, Roth Y, Ochershvilli A et al (2004) Pretreatment prediction of brain tumors' response to radiation therapy using high b-value diffusion-weighted MRI. Neoplasia 6:136–142
11. Chenevert TL, Sundgren PC, Ross BD (2006) Diffusion imaging: insight to cell status and cytoarchitecture. Neuroimaging Clin N Am 16:619–632 viii-ix
12. Oh J, Henry RG, Pirzkall A et al (2004) Survival analysis in patients with glioblastoma multiforme: predictive value of choline-to-*N*-acetylaspartate index, apparent diffusion coefficient, and relative cerebral blood volume. J Magn Reson Imaging 19:546–554
13. Murakami R, Sugahara T, Nakamura H et al (2007) Malignant supratentorial astrocytoma treated with postoperative radiation therapy: prognostic value of pretreatment quantitative diffusion-weighted MR imaging. Radiology 243:493–499
14. Higano S, Yun X, Kumabe T et al (2006) Malignant astrocytic tumors: clinical importance of apparent diffusion coefficient in prediction of grade and prognosis. Radiology 241:839–846
15. Macdonald DR, Cascino TL, Schold SC Jr et al (1990) Response criteria for phase II studies of supratentorial malignant glioma. J Clin Oncol 8:1277–1280
16. Nagane M, Nozue K, Shimizu S et al (2009) Prolonged and severe thrombocytopenia with pancytopenia induced by radiation-combined temozolomide therapy in a patient with newly diagnosed glioblastoma—analysis of O^6-methylguanine-DNA methyltransferase status. J Neurooncol 92:227–232
17. Hegi ME, Diserens AC, Gorlia T et al (2005) MGMT gene silencing and benefit from temozolomide in glioblastoma. N Engl J Med 352:997–1003
18. Nagane M, Kobayashi K, Ohnishi A et al (2007) Prognostic significance of O6-methylguanine-DNA methyltransferase protein expression in patients with recurrent glioblastoma treated with temozolomide. Jpn J Clin Oncol 37:897–906
19. Wong ET, Brem S (2008) Antiangiogenesis treatment for glioblastoma multiforme: challenges and opportunities. J Natl Compr Canc Netw 6:515–522
20. Gerstner ER, Frosch MP, Batchelor TT (2010) Diffusion magnetic resonance imaging detects pathologically confirmed, nonenhancing tumor progression in a patient with recurrent glioblastoma receiving bevacizumab. J Clin Oncol 28:e91–e93
21. Pope WB, Kim HJ, Huo J et al (2009) Recurrent glioblastoma multiforme: ADC histogram analysis predicts response to bevacizumab treatment. Radiology 252:182–189
22. Brandsma D, van den Bent MJ (2009) Pseudoprogression and pseudoresponse in the treatment of gliomas. Curr Opin Neurol 22:633–638
23. Levin VA, Bidaut L, Hou P et al (2011) Randomized double-blind placebo-controlled trial of bevacizumab therapy for radiation necrosis of the central nervous system. Int J Radiat Oncol Biol Phys 79:1487–1495
24. Pope WB, Young JR, Ellingson BM (2011) Advances in MRI assessment of gliomas and response to anti-VEGF therapy. Curr Neurol Neurosci Rep 11:336–344
25. Ellingson BM, Cloughesy TF, Lai A et al (2012) Quantification of edema reduction using differential quantitative T2 (DQT2) relaxometry mapping in recurrent glioblastoma treated with bevacizumab. J Neurooncol 106:111–119
26. Wen PY, Macdonald DR, Reardon DA et al (2010) Updated response assessment criteria for high-grade gliomas: response assessment in neuro-oncology working group. J Clin Oncol 28:1963–1972
27. Pope WB, Lai A, Mehta R et al (2011) Apparent diffusion coefficient histogram analysis stratifies progression-free survival in newly diagnosed bevacizumab-treated glioblastoma. AJNR Am J Neuroradiol 32:882–889

J Neurooncol (2012) 107:147–153
DOI 10.1007/s11060-011-0721-3

CLINICAL STUDY – PATIENT STUDY

O^6-methylguanine-DNA methyltransferase promoter methylation in 45 primary central nervous system lymphomas: quantitative assessment of methylation and response to temozolomide treatment

Jun-ichi Adachi · Kazuhiko Mishima · Kenji Wakiya · Tomonari Suzuki · Kohei Fukuoka · Takaaki Yanagisawa · Masao Matsutani · Atsushi Sasaki · Ryo Nishikawa

Received: 13 June 2011 / Accepted: 17 September 2011 / Published online: 4 October 2011

Abstract Favorable responses to temozolomide chemotherapy have recently been reported in primary central nervous system lymphoma (PCNSL) patients who are refractory to high-dose methotrexate therapy. The gene encoding the DNA repair enzyme O^6-methylguanine-DNA methyltransferase (MGMT) is transcriptionally silenced by promoter methylation in several human tumors, including gliomas and systemic lymphomas. *MGMT* promoter methylation is also a prognostic marker in glioblastoma patients treated with temozolomide. To validate temozolomide treatment in PCNSL, we applied methylation-sensitive high resolution melting (MS-HRM) analysis to quantitate *MGMT* methylation in PCNSL. *MGMT* promoter methylation was detected in tumors from 23 (51%) of 45 PCNSL patients, 11 of which were considered to have high (more than 70.0%) methylation status. Of the five recurrent PCNSLs treated with temozolomide, four cases responded, with three achieving complete response and one, a partial response. All four responsive PCNSLs had methylated *MGMT* promoters, whereas the non-responsive recurrent PCNSL did not. Thus, the use of quantitative MS-HRM analysis for the detection of *MGMT* promoter methylation has been suggested in PCNSL for the first time. The assay allows rapid and high-throughput evaluation of the *MGMT* methylation status, and seems to be promising in clinical settings. *MGMT* promoter methylation may become a useful marker for predicting the response of PCNSLs to temozolomide.

Keywords Primary central nervous system lymphoma · MGMT · Temozolomide · Chemotherapy

J. Adachi (✉) · K. Mishima · K. Wakiya · T. Suzuki · K. Fukuoka · T. Yanagisawa · M. Matsutani · R. Nishikawa
Department of Neuro-Oncology/Neurosurgery, Comprehensive Cancer Center, Saitama Medical University International Medical Center, 1397-1 Yamane, Hidaka-shi, Saitama 350-1298, Japan
e-mail: jadachi@saitama-med.ac.jp

A. Sasaki
Department of Pathology, Saitama Medical University, 38 Morohongo, Moroyama-machi, Iruma-gun, Saitama 350-0495, Japan

Introduction

Primary central nervous system lymphoma (PCNSL) is characterized by rapid progression, frequent cerebrospinal fluid involvement, and early recurrence [1]. The introduction of combined pre-irradiation high-dose methotrexate (HD-MTX) with radiation therapy has resulted in a median survival time of 33 months [2, 3]. HD-MTX, however, is associated with considerable systemic toxicity affecting renal, cardiac, and hematological function [4]. There are also important limitations of radiation therapy, including an increased risk of late neurotoxicity, especially in elderly patients [5]. Thus, there is a need for an alternative chemotherapy that is both efficient and well-tolerated. Cyclophosphamide–adriamycin–vincristine–prednisolone (CHOP) chemotherapy is the standard chemotherapy for systemic malignant lymphoma, but the drugs do not penetrate the brain effectively and do not improve survival of patients with PCNSL [6, 7]. Temozolomide is an alkylating agent with good cerebrospinal fluid penetration [8], and there have been some reports of temozolomide efficacy with acceptable toxicity in cases of PCNSL [9–12].

Previous studies on glioma and systemic lymphoma associated the presence of the methylated form of the O^6-methylguanine-DNA methyltransferase (*MGMT*) gene

with a more favorable response to alkylating agents [13–15]. MGMT is a DNA repairing enzyme that removes alkyl adducts from the O^6 position of guanine and prevents the cytotoxic, mutagenic, and carcinogenic effects of alkylating agents such as temozolomide [16–19]. It has been demonstrated that silencing of *MGMT* is involved in carcinogenesis in humans [20, 21]. The loss of *MGMT* function in human cancer cells is mainly due to the hypermethylation of CpG islands in the gene's promoter sequence [22, 23]. Therefore, evaluation of the methylation status of the *MGMT* promoter is important to validate temozolomide treatment in PCNSL.

In this study, we applied, for the first time, methylation-sensitive high resolution melting (MS-HRM) analysis to quantify the *MGMT* methylation status in 45 cases of PCNSL. In addition, the *MGMT* methylation level was compared with the clinical response to temozolomide treatment.

Patients and methods

Patients and treatment

We studied 45 patients with newly diagnosed PCNSL between 2002 and 2011. Tumor samples were obtained by surgical resection or biopsy prior to therapy. On the basis of pathological examination, a diagnosis of diffuse large B cell lymphoma was made in all cases. Written informed consent for use of their tissues was obtained from study subjects.

The primary treatment was high-dose methotrexate (HD-MTX)-based chemotherapy in 43 patients, and exclusive radiation therapy (RT) in one patient, and one patient received no adjuvant treatment after surgery. The MTX dose was 1–3.5 g/m^2. MTX was used as a single agent in 15 patients, and was combined with 375 mg/m^2 rituximab in 28 patients. After primary chemotherapy, RT was performed in 32 of 43 cases. The remaining 11 cases were patients older than 65 years, and were treated without RT to avoid cognitive dysfunction due to radiation-induced leukoencephalopathy. We continued HD-MTX-based chemotherapy for these 11 patients until the tumor progressed.

Fourteen patients received oral temozolomide at 150–200 mg/m^2 per day for 5 days every 4 weeks (Table 1). Five (cases 1–5) of 14 cases were treated with temozolomide as salvage chemotherapy upon relapse after standard HD-MTX/radiation therapy. For the remaining nine patients (cases 6–14), temozolomide was used as adjuvant chemotherapy after first-line HD-MTX therapy.

DNA extraction and *MGMT* quantitative methylation assay

Genomic DNA was extracted from fresh frozen (43 of 45 cases) or paraffin-embedded formalin-fixed (2 of 45 cases)

Table 1 Summary of 14 PCNSL patients treated with temozolomide

Case No.	Age at temozolomide treatment (years)/ gender	No. of temozolomide cycles[a]	Maximum response to temozolomide	Duration (months) keeping CR or PR	Therapy prior to temozolomide treatment	Degree of *MGMT* promoter methylation[b]
1	75/M	19	CR	38	M, R, RT	61.7 ± 4.04
2	60/M	3	CR	12	M, R, RT	99.0 ± 1.00
3	47/M	5	PR	7	M, R, RT	72.3 ± 2.52
4	72/M	2	PD		M, R, RT	1.3 ± 1.26
5	50/M	8	CR	7	M, R, ICE, RT	94.3 ± 2.50
6	64/F	2	CR	11	M	7.7 ± 0.58
7	73/F	6	CR	11	M, RT	0.8 ± 0.96
8	70/M	5	CR	21	M, RT	1.5 ± 1.28
9	55/M	4	CR	27	M, R, RT	26.7 ± 0.58
10	57/M	3	CR	24	M, R, RT	1.8 ± 0.96
11	54/M	3	PD		M, R, RT	32.0 ± 1.83
12	62/F	2	CR	24	M, R, RT	0.3 ± 0.50
13	72/M	10	PR	9	M, R, RT	1.0 ± 0.82
14	85/F	9	CR	7	M, R	74.7 ± 0.58

Cases 1–5 were treated with temozolomide as salvage chemotheapy at relapse after standard HD-MTX/radiation therapy. Cases 6–14 were treated with adjuvant temozolomide therapy after first-line HD-MTX therapy

CR complete response; *PR* partial response; *PD* progressive disease

M HD-MTX; *R* rituximab; *ICE* Ifosfamide + Cisplatin + Etoposide; *RT* radiation therapy

[a] Patients received oral temozolomide for 5 days every 4 weeks

[b] Percentage of *MGMT* methylation level in our assay. The mean ± standard deviation is indicated

Table 2 The primers designed to target the promoter sequences of the *MGMT* gene

	Primer sequences 5′–3′
MGMT MS-HRM[a]	F-GCGTTTCGGATATGTTGGGATAGT
	R-CCTACAAAACCACTCGAAACTACCA

[a] Methylation-sensitive high-resolution melting

brain biopsy specimens using the DNeasy Tissue kit (Qiagen, Hilden, Germany) according to the manufacturer's protocol.

We quantified the methylation status of the *MGMT* promoter's CpG-rich region using MS-HRM analysis [24]. Briefly, 500 ng of genomic DNA was treated with sodium bisulfite using the Epitect Bisulfite Kit (Qiagen, Hilden, Germany) according to the manufacturer's instructions. PCR amplification and MS-HRM analysis were carried out sequentially on a LightCycler480 real-time PCR system (Roche Diagnostics, Mannheim, Germany). The primer sets to amplify 18 CpG-rich sites in the *MGMT* promoter were designed according to previous reports (Table 2) [24, 25]. Each PCR run contained 2 μl of bisulfite-converted DNA in a total volume of 20 μl: 2× master mix containing high-resolution melting dye (Roche Diagnostics, Mannheim, Germany), 4 mM Mg^{2+}, and 500 nM of each primer. Cycling conditions were 10 min at 95°C, followed by 45 cycles of denaturation at 95°C for 15 s, annealing at 60°C for 20 s, and extension at 60°C for 20 s. The melting step was 95°C for 1 min, 50°C for 1 min, 72°C for 5 s, and continuous acquisition to 95°C at 30 acquisitions per 1°C. As positive (100% methylated) and negative (0% methylated) controls, we used CpGenome™ Universal Methylated and Unmethylated DNA (Chemicon, Millipore, Billerica, MA), respectively. The duration of the run from the onset of PCR was approximately 80 min. All reactions were performed at least in triplicate.

Methylation-specific polymerase chain reaction (MSP)

Bisulfite-treated DNA was also subjected to MSP assay of *MGMT* promoter methylation in 14 PCNSL patients treated with temozolomide. We developed nested PCR using primers described in Esteller et al. and Palmisano et al. [23, 27]. The first round of PCR was performed to amplify a 289 bp fragment of the *MGMT* gene including a portion of their CpG-rich promoter region. Primer sequences used in the first round amplification are as follows: 5′-GGA TATGTTGGGATAGTT-3′ (sense) and 5′-CCAAAAACC CCAAACCC-3′ (antisence). 5 μl of the first round PCR products was subjected to the second round PCR in which primers specific to methylated or unmethylated template. A 93 bp unmethylated product was amplified using the primers: 5′-TTTGTGTTTTGATGTTTGTAGGTTTTTG T-3′ (sense) and 5′-AACTCC AACACTCTTCCAAA AACAAAACA-3′ (antisense). An 81 bp methylated product was amplified using the following primers: 5′-TTT CGACGTTCGTAGGTTTTCGC-3′ (sense) and 5′-GCAC TCTTCCGAAAACGAAACG-3′ (antisense). The PCR mixture contained 5 μl DNA, 10× PCR Buffer (TaKaRa), 5 nmol each deoxynucleotide, 2.5 pmol of each primer and 0.8 U *Taq* HS (TaKaRa), in a final volume of 50 μl. The first round PCR cycling conditions were as follows: 95°C for 10 min, then denature at 95°C for 30 s, anneal at 52°C for 30 s, extension at 72°C for 30 s for 40 cycles followed by a 10 min final extension. In the second round PCR, annealing temperature was increased to 62°C and all of the cycling times were reduced to 15 s for a total of 34 cycles. An aliquot of 10 μl of the second round PCR was loaded onto a 12.5% polyacrylamide gel, stained with ethidium bromide and visualized under UV illumination.

Results

Melting data collected using the LightCycler480 Instrument can be analyzed by the "Tm (Melting Temperature) calling" algorithm that converts the melting profiles into derivative plots, which allows methylated and unmethylated samples to be distinguished. Products amplified from methylated DNA have a higher Tm due to the presence of CpGs in the amplicon. In contrast, products amplified from unmethylated DNA have a low Tm due to the conversion of unmethylated cytosine to uracil in the bisulfite-modified DNA sample, which results in thymine in the amplicon. If the sample contains a mixture of methylated and unmethylated DNA, two peaks are displayed, as shown in Fig. 1. This assay was able to detect 1.0% methylated DNA over a background of unmethylated DNA. We used the LightCycler480 Gene Scanning Software ver.1.5 to generate standard curves for methylated *MGMT* using serial samples having known ratios of methylated to unmethylated template. The *MGMT* methylation level of an unknown sample could then be estimated from these standard curves. The samples were analyzed at least in triplicates, and we determined the methylation levels from the average value of the experiments. A cut-off value of 4.0% methylated *MGMT* was previously validated by strong correlation of protein expression loss with MGMT promoter methylation [26]. Therefore, samples with an average *MGMT* methylation level of less than 4.0% were defined as unmethylated.

Of the 45 PCNSLs examined by MS-HRM assay, all samples were amplifiable and gave interpretable results. The *MGMT* promoter was methylated in 23 PCNSLs (51%), and was unmethylated in the remaining 22 cases

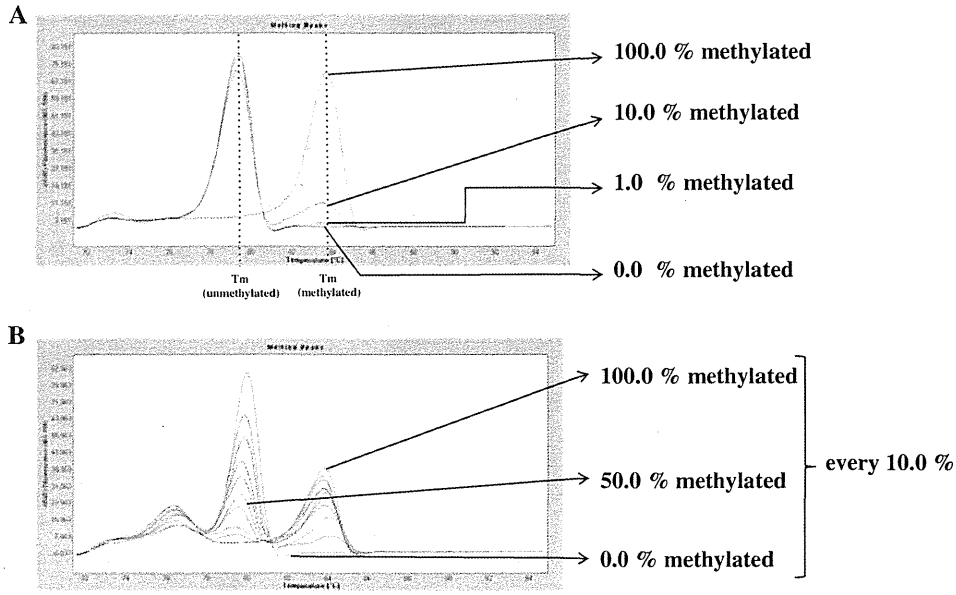

Fig. 1 **A** *MGMT* methylation-sensitive high-resolution melting (MS-HRM) analysis with 100.0% methylated, 0.0% methylated controls, and methylation standards at 10.0 and 1.0% in 0.0% methylated background. Data were analyzed using the Tm calling software module. Two different peaks are obtained for the PCR product derived from the methylated and unmethylated templates. The samples containing a mixture of methylated and unmethylated DNA (methylation standards at 10.0 and 1.0% in 0.0% methylated background) display two peaks. Tm (unmethylated), melting temperature derived from unmethylated DNA; Tm (methylated), melting temperature derived from methylated DNA. **B** *MGMT* MS-HRM analysis with 100.0% methylated, 0.0% methylated, and serially diluted standards at every 10.0%. Data were analyzed using the Tm calling software module

(Table 3). The average methylation level in the 23 methylated samples ranged from 4.1 to 100%. Tumors with a high methylation status (more than 70.0% methylated) were detected in 11 (48%) of the 23 *MGMT*-methylated cases.

Four of five patients with recurrent PCNSLs responded to temozolomide treatment; two cases had a complete response (CR) over 12 months after 1 or 2 cycles of temozolomide, two patients had a partial response (PR), and the remaining patient had progressive disease (Fig. 2). Tumors of all four responders showed relatively high methylation (61.7–99.0%) of the *MGMT* gene (Table 1), and significant *MGMT* methylation was not detected in the patient with progressive disease. In MSP, both unmethylated and methylated *MGMT* were detected in all patients including three cases demonstrated in Fig. 3. It was quite difficult to evaluate the degree of *MGMT* methylation from the result of MSP.

Of the nine cases treated with adjuvant temozolomide after first-line HD-MTX therapy, eight achieved a CR or PR of 7 to 27 months with temozolomide. In addition to HD-MTX and temozolomide, these nine patients received differing treatments (rituximab plus RT in five patients, RT in two patients, rituximab in one patient, and none in one patient). Therefore, we did not investigate the relationship between survival time and methylation status in the patients receiving adjuvant temozolomide.

Table 3 Methylation status of the *MGMT* promoter in 45 PCNSL patients

Degree of *MGMT* promoter methylation (%)[a]	No.
<4.0 (=unmethylated cases)	22
4.1–9.9	3
10.0–19.9	1
20.0–29.9	2
30.0–39.9	2
40.0–49.9	2
50.0–59.9	0
60.0–69.9	2
70.0–79.9	4
80.0–89.9	2
90.0–100.0	5

[a] Percentage of *MGMT* methylation level in our assay

Discussion

The *MGMT* gene is known to be methylated in some systemic B-cell lymphomas [15, 28, 29], but to our knowledge, there has been only one report of *MGMT* methylation in PCNSL[30]. In that study, 6 (60%) of 10 assessable PCNSL patients had methylated MGMT promoters, as measured by gel-based MSP, which is a highly sensitive method to determine epigenetic silencing of genes. As shown in our MSP assay, MSP can detect very low levels

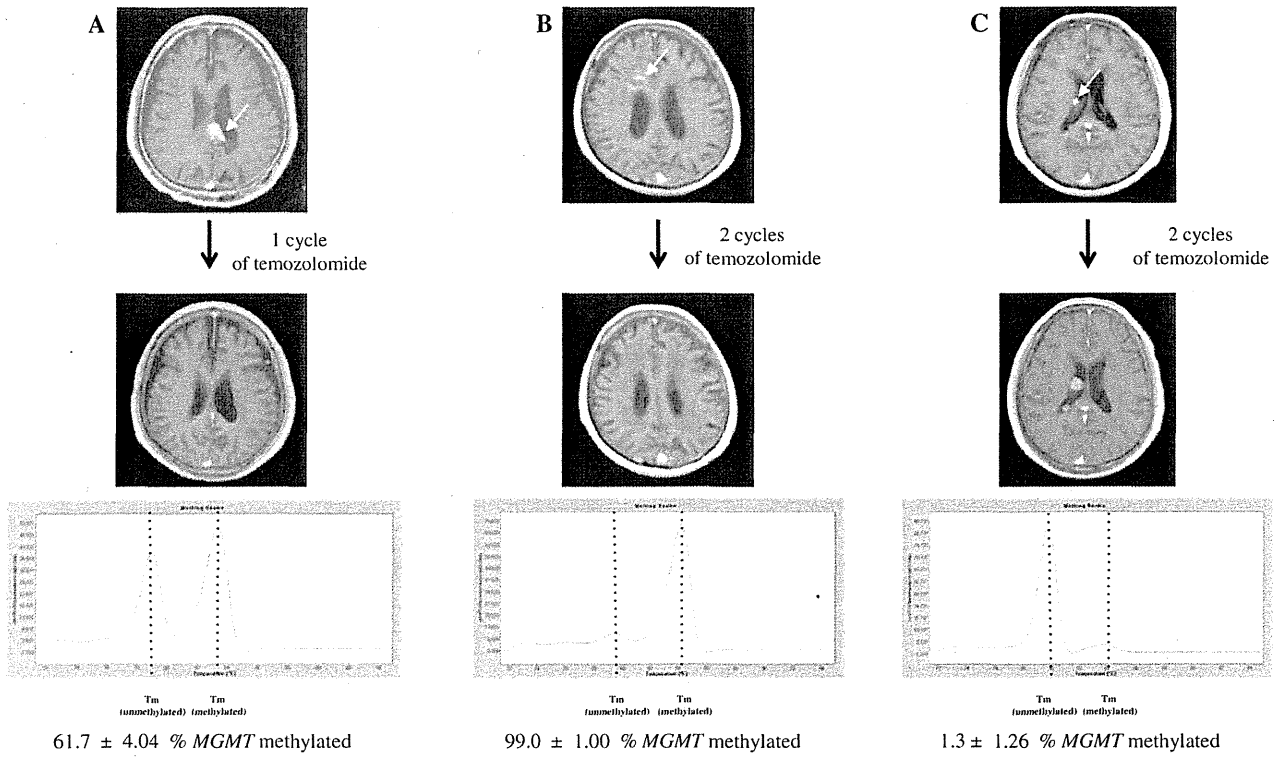

Fig. 2 Relapsed PCNSL cases treated with temozolomide as salvage chemotherapy. **A–C** are cases 1, 2, and 4 in Table 1, respectively. Upper panels show gadolinium-enhanced T1-weighted magnetic resonance images before and after temozolomide treatment. The *white arrows* indicate relapsed tumors. After chemotherapy, tumors completely disappeared in cases 1 and 2, whereas the tumor progressed in case 4. Lower panels show the representative profile of *MGMT* methylation in each case. The mean percentage ± standard deviation of *MGMT* methylation is indicated at the *bottom*

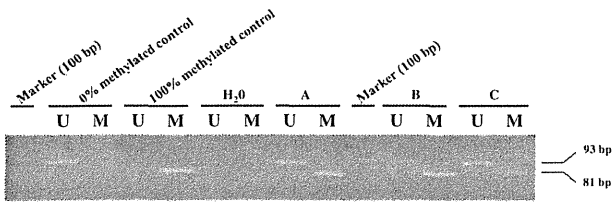

Fig. 3 Methylation-specific PCR results of *MGMT* promoter in cases shown in Fig. 2. PCR products in *lanes* marked as (*U*) indicate the presence of unmethylated *MGMT* alleles. PCR products in *lanes* marked as (*M*) indicate the presence of methylated *MGMT* alleles. 0% methylated control was used as a negative control for methylation, 100% methylated control was used as a positive control for methylation, and water (H_2O) was used as negative PCR control. Marker is a 100 bp DNA marker. The sizes of PCR products are indicated on the right scale. **A–C** are cases 1, 2, and 4 in Table 1, respectively

of DNA methylation or unmethylation. However, several recent studies have raised serious concerns about the application of MSP in a clinical setting. Because of the qualitative nature of the assay, MSP cannot distinguish between high levels of methylation and low levels that have little or no biological significance. Ogino et al. [26] showed that MGMT protein expression was not silenced in tumors with low levels of methylation (less than 4%) in the *MGMT* promoter . Uccella et al. [29] demonstrated that the *MGMT* methylation status correlated with survival in systemic B-cell lymphoma patients treated with alkylating agents; the outcome of survival analysis was unfavorable both in patients with less than 4.0% *MGMT* methylation and in patients with fully unmethylated tumors. Our assay identified some cases with negligible methylation (less than 4.0%), which should have been considered as unmethylated but were defined as methylated by the MSP method. Therefore, it seems reasonable that the *MGMT* methylation frequencies in our series were slightly lower than that found in a previous study using MSP [30]. In addition, a recent study suggested that the MSP assay for *MGMT* methylation is not sufficiently reproducible to make it suitable for clinical use [31]. Thus, a quantitative assay should be used to evaluate *MGMT* promoter methylation in clinical settings. Our study is the first to quantify *MGMT* methylation levels in 45 PCNSLs, which is the largest number of samples reported so far.

Salvage temozolomide treatment has been effective for PCNSL patients who experienced a relapse after HD-MTX chemotherapy. Although cases were small in number, our

results indicate that temozolomide was especially beneficial to patients with tumors containing a highly methylated *MGMT* promoter. Methylation of the *MGMT* promoter is a strong predictor of response, overall survival, and time to disease progression in glioblastoma patients treated with temozolomide [13]. Both the *MGMT* methylation frequency and the proportion of highly methylated tumors are significantly higher for PCNSL than for glioblastoma (our unpublished data), which may explain why PCNSL patients responded to temozolomide. An analysis of more PCNSL patients is needed to evaluate the predictive power of *MGMT* methylation on the impact of salvage temozolomide treatment in PCNSL. Adjuvant therapy with temozolomide is also promising, and a phase III study on the use of HD-MTX and whole brain radiotherapy, with or without concomitant and adjuvant temozolomide, in PCNSL patients is being planned by the Japan Clinical Oncology Group Brain Tumor Study Group.

Acknowledgments This work was supported by a Grant-in-Aid for Scientific Research (C) from the Japan Society for the Promotion of Science (JSPS), 2008–2010. We thank Ms. Kyoko Totake and Mr. Makoto Yamashiro for their technical assistance.

References

1. Herrlinger U, Schabet M, Brugger W, Kortmann RD, Küker W, Deckert M, Engel C, Schmeck-Lindenau HJ, Mergenthaler HG, Krauseneck P, Benöhr C, Meisner C, Wiestler OD, Dichgans J, Kanz L, Bamberg M, Weller M (2002) German Cancer Society Neuro-Oncology Working Group NOA-03 multicenter trial of single-agent high-dose methotrexate for primary central nervous system lymphoma. Ann Neurol 51:247–252
2. Glass J, Gruber ML, Cher L, Hochberg FH (1994) Preirradiation methotrexate chemotherapy of primary central nervous system lymphoma: long-term outcome. J Neurosurg 81:188–195
3. O'Brien P, Roos D, Pratt G, Liew K, Barton M, Poulsen M, Olver I, Trotter G (2000) Phase II multicenter study of brief single-agent methotrexate followed by irradiation in primary CNS lymphoma. J Clin Oncol 18:519–526
4. Treon SP, Chabner BA (1996) Concepts in use of high-dose methotrexate therapy. Clin Chem 42:1322–1329
5. Hoang-Xuan K, Taillandier L, Chinot O, Soubeyran P, Bogdhan U, Hildebrand J, Frenay M, De Beule N, Delattre JY, Baron B, European Organization for Research, Treatment of Cancer Brain Tumor Group (2003) Chemotherapy alone as initial treatment for primary CNS lymphoma in patients older than 60 years: a multicenter phase II study (26952) of the European Organization for Research and Treatment of Cancer Brain Tumor Group. J Clin Oncol 21:2726–2731
6. O'Neill BP, O'Fallon JR, Earle JD, Colgan JP, Brown LD, Krigel RL (1995) Primary central nervous system non-Hodgkin's lymphoma: survival advantages with combined initial therapy? Int J Radiat Oncol Biol Phys 33:663–673
7. Schultz C, Scott C, Sherman W, Donahue B, Fields J, Murray K, Fisher B, Abrams R, Meis-Kindblom J (1996) Preirradiation chemotherapy with cyclophosphamide, doxorubicin, vincristine, and dexamethasone for primary CNS lymphomas: initial report of radiation therapy oncology group protocol 88-06. J Clin Oncol 14:556–564
8. Newlands ES, Stevens MF, Wedge SR, Wheelhouse RT, Brock C (1997) Temozolomide: a review of its discovery, chemical properties, pre-clinical development and clinical trials. Cancer Treat Rev 23:35–61
9. Herrlinger U, Küker W, Platten M, Dichgans J, Weller M (2002) First-line therapy with temozolomide induces regression of primary CNS lymphoma. Neurology 58:1573–1574
10. Lerro KA, Lacy J (2002) Case report: a patient with primary CNS lymphoma treated with temozolomide to complete response. J Neurooncol 59:165–168
11. Omuro AM, Taillandier L, Chinot O, Carnin C, Barrie M, Hoang-Xuan K (2007) Temozolomide and methotrexate for primary central nervous system lymphoma in the elderly. J Neurooncol 85:207–211
12. Reni M, Zaja F, Mason W, Perry J, Mazza E, Spina M, Bordonaro R, Ilariucci F, Faedi M, Corazzelli G, Manno P, Franceschi E, Pace A, Candela M, Abbadessa A, Stelitano C, Latte G, Ferreri AJ (2007) Temozolomide as salvage treatment in primary brain lymphomas. Br J Cancer 96:864–867
13. Hegi ME, Diserens AC, Gorlia T, Hamou MF, de Tribolet N, Weller M, Kros JM, Hainfellner JA, Mason W, Mariani L, Bromberg JE, Hau P, Mirimanoff RO, Cairncross JG, Janzer RC, Stupp R (2005) MGMT gene silencing and benefit from temozolomide in glioblastoma. N Engl J Med 352:997–1003
14. Everhard S, Kaloshi G, Crinière E, Benouaich-Amiel A, Lejeune J, Marie Y, Sanson M, Kujas M, Mokhtari K, Hoang-Xuan K, Delattre JY, Thillet J (2006) MGMT methylation: a marker of response to temozolomide in low-grade gliomas. Ann Neurol 60:740–743
15. Esteller M, Gaidano G, Goodman SN, Zagonel V, Capello D, Botto B, Rossi D, Gloghini A, Vitolo U, Carbone A, Baylin SB, Herman JG (2002) Hypermethylation of the DNA repair gene O(6)-methylguanine DNA methyltransferase and survival of patients with diffuse large B-cell lymphoma. J Natl Cancer Inst 94:26–32
16. Margison GP, Santibanez-Koref MF (2002) O^6-alkylguanine-DNA alkyltransferase: role in carcinogenesis and chemotherapy. Bioessays 24:255–256
17. Gerson SL (2004) MGMT: its role in cancer aetiology and cancer therapeutics. Nat Rev Cancer 4:296–307
18. Karran P, Bignami M (1994) DNA damage tolerance, mismatch repair and genome instability. Bioessays 16:833–839
19. Gerson SL (2002) Clinical relevance of MGMT in the treatment of cancer. J Clin Oncol 20:2388–2399
20. Becker K, Gregel CM, Kaina B (1997) The DNA repair protein O^6-methylguanine-DNA methyltransferase protects against skin tumor formation induced by antineoplastic chloroethylnitrosourea. Cancer Res 57:3335–3338
21. Sakumi K, Shiraishi A, Shimizu S, Tsuzuki T, Ishikawa T, Sekiguchi M (1997) Methylnitrosourea-induced tumorigenesis in MGMT gene knockout mice. Cancer Res 57:2415–2418
22. Danam RP, Qian Howell SR, Brent TP (1999) Methylation of selected CpGs in the human O^6-methylguanine-DNA methyltransferase promoter region as a marker of gene silencing. Mol Carcinog 24(2):85–89
23. Esteller M, Hamilton SR, Burger PC, Baylin SB, Herman JG (1999) Inactivation of the DNA repair gene O^6-methylguanine-DNA methyltransferase by promoter hypermethylation is a common event in primary human neoplasia. Cancer Res 59:793–797
24. Wojdacz TK, Hansen LL (2006) Reversal of PCR bias for improved sensitivity of the DNA methylation melting curve assay. Biotechniques 41:274–278

25. Wojdacz TK, Dobrovic A (2007) Methylation-sensitive high resolution melting (MS-HRM): a new approach for sensitive and high-throughput assessment of methylation. Nucleic Acids Res 35:e41
26. Ogino S, Kawasaki T, Brahmandam M, Cantor M, Kirkner GJ, Spiegelman D, Makrigiorgos GM, Weisenberger DJ, Laird PW, Loda M, Fuchs CS (2006) Precision and performance characteristics of bisulfite conversion and real-time PCR (MethyLight) for quantitative DNA methylation analysis. J Mol Diagn 8:209–217
27. Palmisano WA, Divine KK, Saccomanno G, Gilliland FD, Baylin SB, Herman JG, Belinsky SA (2000) Predicting lung cancer by detecting aberrant promoter methylation in sputum. Cancer Res 60:5954–5958
28. Pike BL, Greiner TC, Wang X, Weisenburger DD, Hsu YH, Renaud G, Wolfsberg TG, Kim M, Weisenberger DJ, Siegmund KD, Ye W, Groshen S, Mehrian-Shai R, Delabie J, Chan WC, Laird PW, Hacia JG (2008) DNA methylation profiles in diffuse large B-cell lymphoma and their relationship to gene expression status. Leukemia 22:1035–1043
29. Uccella S, Cerutti R, Placidi C, Marchet S, Carnevali I, Bernasconi B, Proserpio I, Pinotti G, Tibiletti MG, Furlan D, Capella C (2009) MGMT methylation in diffuse large B-cell lymphoma: validation of quantitative methylation-specific PCR and comparison with MGMT protein expression. J Clin Pathol 62:715–723
30. Kurzwelly D, Glas M, Roth P, Weimann E, Lohner H, Waha A, Schabet M, Reifenberger G, Weller M, Herrlinger U (2009) Primary CNS lymphoma in the elderly: temozolomide therapy and MGMT status. J Neurooncol 97:389–392
31. Vlassenbroeck I, Califice S, Diserens AC, Migliavacca E, Straub J, Di Stefano I, Moreau F, Hamou MF, Renard I, Delorenzi M, Flamion B, DiGuiseppi J, Bierau K, Hegi ME (2008) Validation of real-time methylation-specific PCR to determine O^6-methylguanine-DNA methyltransferase gene promoter methylation in glioma. J Mol Diagn 10:332–337

Phosphorylation of dedicator of cytokinesis 1 (Dock180) at tyrosine residue Y722 by Src family kinases mediates EGFRvIII-driven glioblastoma tumorigenesis

Haizhong Feng[a,b], Bo Hu[a,c,1], Michael J. Jarzynka[a,b,2], Yanxin Li[d], Susan Keezer[e], Terrance G. Johns[f], Careen K. Tang[g], Ronald L. Hamilton[b], Kristiina Vuori[h], Ryo Nishikawa[i], Jann N. Sarkaria[j], Tim Fenton[k,3], Tao Cheng[d,l], Frank B. Furnari[k], Webster K. Cavenee[k,1], and Shi-Yuan Cheng[a,b,1]

[a]University of Pittsburgh Cancer Institute, Departments of [b]Pathology, [c]Medicine, and [d]Radiation Oncology, University of Pittsburgh School of Medicine, Pittsburgh, PA 15213; [e]Cell Signaling Technology, Inc., Danvers, MA 01923; [f]Oncogenic Signaling Laboratory, Monash Institute of Medical Research, Clayton, Victoria 3168, Australia; [g]Department of Oncology, Lombardi Comprehensive Cancer Center, Georgetown University Medical Center, Washington, DC 20057; [h]Cancer Center, Sanford-Burnham Medical Research Institute, La Jolla, CA 92037; [i]Department of Neurosurgery, Saitama Medical University, Saitama 350-0495, Japan; [j]Department of Radiation Oncology, Mayo Clinic, Rochester, MN 55905; [k]Ludwig Institute for Cancer Research, University of California at San Diego School of Medicine, La Jolla, CA 92093; and [l]State Key Laboratory of Experimental Hematology, Institute of Hematology and Blood Diseases Hospital, Center for Stem Cell Medicine, Chinese Academy of Medical Sciences and Peking Union Medical College, Tianjin 300041, China

Contributed by Webster K. Cavenee, December 29, 2011 (sent for review November 30, 2011)

Glioblastoma, the most common primary malignant cancer of the brain, is characterized by rapid tumor growth and infiltration of tumor cells throughout the brain. These traits cause glioblastomas to be highly resistant to current therapies with a resultant poor prognosis. Although aberrant oncogenic signaling driven by signature genetic alterations, such as EGF receptor (EGFR) gene amplification and mutation, plays a major role in glioblastoma pathogenesis, the responsible downstream mechanisms remain less clear. Here, we report that EGFRvIII (also known as ΔEGFR and de2-7EGFR), a constitutively active EGFR mutant that is frequently co-overexpressed with EGFR in human glioblastoma, promotes tumorigenesis through Src family kinase (SFK)-dependent phosphorylation of Dock180, a guanine nucleotide exchange factor for Rac1. EGFRvIII induces phosphorylation of Dock180 at tyrosine residue 722 (Dock180^{Y722}) and stimulates Rac1-signaling, glioblastoma cell survival and migration. Consistent with this being causal, siRNA knockdown of Dock180 or expression of a Dock180^{Y722F} mutant inhibits each of these EGFRvIII-stimulated activities. The SFKs, Src, Fyn, and Lyn, induce phosphorylation of Dock180^{Y722} and inhibition of these SFKs by pharmacological inhibitors or shRNA depletion markedly attenuates EGFRvIII-induced phosphorylation of Dock180^{Y722}, Rac1 activity, and glioblastoma cell migration. Finally, phosphorylated Dock180^{Y722} is coexpressed with EGFRvIII and phosphorylated Src^{Y418} in clinical specimens, and such coexpression correlates with an extremely poor survival in glioblastoma patients. These results suggest that targeting the SFK-p-Dock180^{Y722}-Rac1 signaling pathway may offer a novel therapeutic strategy for glioblastomas with EGFRvIII overexpression.

invasion | Akt

Oncogenic signaling stimulated by overexpressed genes, such as EGF receptor (EGFR), renders human brain glioblastomas malignant and resistant to combination therapies (1). Amplification of EGFR is the most frequent genetic alteration in World Health Organization (WHO) grade IV glioblastoma multiforme (GBM) (2, 3) and is associated with poor prognosis (1). About half of GBMs with EGFR amplification also express the mutant form, EGFRvIII/ΔEGFR/de2-7EGFR, that lacks a portion of the extracellular ligand-binding domain (encoded by exons 2 through 7), leading to constitutively activated oncogenic signaling (3, 4). Expression of EGFRvIII enhances glioblastoma tumorigenicity in vivo (5) and promotes glioblastoma cell motility in vitro (6). Although EGFRvIII activates PI3K/Akt signaling, other signaling cascades are also likely involved in mediating EGFRvIII-driven tumorigenesis (3, 4).

Dedicator of cytokinesis 1 (Dock1 or Dock180) is a guanine nucleotide exchange factor (GEF) that activates Rac1 and controls several cellular functions, including cell motility, survival, and proliferation (7). Dock180 facilitates nucleotide exchange on Rac1 through its Dock-homology region-2 (DHR-2) domain, but requires binding to engulfment and cell motility protein 1 (ELMO1) through its N-terminal SH3 domain to achieve full activation of Rac1 (8). Adjacent to the SH3 region resides a DHR-1 domain which interacts with phosphatidyl-inositol(3,4,5)P_3 (PIP_3), and thereby mediates the localization of Dock180 to the cell membrane sites of PIP_3 production where Dock180 subsequently activates Rac1 through its DHR-2 domain (8). Although genomic studies have revealed no genetic alterations in Rac1, Dock180, or ELMO1 in various human cancers, including glioblastoma, it remains possible, given its central role in regulating cellular functions, that GEF-Rac1 signaling is stimulated by signals emanating from activated oncogenes, such as EGFRvIII.

GEF activation by receptor tyrosine kinases (RTK) stimulates Rac1 (9) and may be important in EGFRvIII-driven tumorigenesis (3). Dock180 activates Rac1 (8) and is involved in RTK-induced cell migration in *Drosophila* (10), and Dock180 plays a role in glioblastoma cell invasion through the activation of Rac1 (11). Here, we report that EGFRvIII induces tyrosine phosphorylation (p-Y) at tyrosine residue 722 (Y722) of Dock180, and that Dock180 and its phosphorylation are required for EGFRvIII-promoted glioblastoma cell growth, survival, and invasion. Correspondingly, ectopic expression of an unphosphorylatable Dock180^{Y722F} mutant inhibited EGFRvIII-induced Rac1 activation, cell migration, and survival in vitro, and glioblastoma growth and invasion in the brain. We also report that EGFRvIII-induced p-Dock180^{Y722} is dependent on Src family kinases (SFKs), that p-Dock180^{Y722} is coexpressed with EGFRvIII and pan-p-Src^{Y418} in clinical glioblastoma specimens, and that such coexpression correlates with an extremely poor prognosis.

Results

Dock180 Is Required for EGFRvIII-Promoted Glioblastoma Cell Migration and Survival in Vitro. To determine if EGFRvIII signaling engages Dock180 as part of its oncogenic mechanism, we

Author contributions: H.F., B.H., and S.-Y.C. designed research; H.F., B.H., M.J.J., and Y.L. performed research; S.K., T.G.J., C.K.T., R.L.H., K.V., R.N., J.N.S., T.F., T.C., F.B.F., and W.K.C. contributed new reagents/analytic tools; H.F., B.H., and S.-Y.C. analyzed data; and H.F., B.H., F.B.F., W.K.C., and S.-Y.C. wrote the paper.

The authors declare no conflict of interest.

[1]To whom correspondence may be addressed. E-mail: hub@upmc.edu, wcavenee@ucsd.edu, or chengs@upmc.edu.

[2]Present Address: Department of Pharmacy, University of Pittsburgh Medical Center-Chartwell, Pittsburgh, PA 15205.

[3]Present Address: Laboratory of Viral Oncology, University College London Cancer Institute, London WC1E 6BT, England.

This article contains supporting information online at www.pnas.org/lookup/suppl/doi:10.1073/pnas.1121457109/-/DCSupplemental.

stably expressed exogenous EGFRvIII in glioblastoma LN444/GFP and SNB19/GFP cells that have high levels of endogenous Dock180 (11). Expression of EGFRvIII in LN444 and SNB19 glioblastoma cells induced p-EGFRvIII, p-Akt, p-Erk1/2, and Rac1 activity (Fig. 1*A*), increased in vitro cell migration (Fig. 1*B*), proliferation (Fig. S1 *A* and *B*), and markedly inhibited cell apoptosis (Fig. S1*C*).

We recently reported that Dock180 promotes glioblastoma cell invasion through activation of Rac1 (11). To determine whether this function of Dock180 is required for EGFRvIII-stimulated glioblastoma tumorigenesis, we knocked down endogenous Dock180 using siRNAs (11) in each of LN444/GFP, LN444/GFP/EGFRvIII, SNB19/GFP, and SNB19/GFP/EGFRvIII cells. As shown in Fig. 1*C*, knockdown of Dock180 in EGFRvIII-expressing cells inhibited EGFRvIII-induced p-Akt, p-Erk1/2, and Rac1 activity. Depletion of Dock180 also suppressed basal Rac1 activity in GFP control cells (11). Knockdown of Dock180 attenuated EGFRvIII-promoted cell migration and survival in EGFRvIII-expressing cells and basal levels of cell migration in GFP control cells (Fig. 1 *D* and *E*). However, depletion of Dock180 had only moderate effects on cell proliferation in both EGFRvIII- and GFP-expressing cells (Fig. 1 *F* and *G*). These data suggest that Dock180 is critical for EGFRvIII-stimulated p-Akt, p-Erk1/2, and Rac1 activity, as well as for glioblastoma cell migration and survival in vitro.

EGFRvIII Induces p-Y of Dock180 at Y722. We examined whether EGFRvIII phosphorylates Dock180 at Y residues in glioblastoma cells. As shown in Fig. 2*A*, p-Y of endogenous Dock180 was evident in both LN444/EGFRvIII and SNB19/EGFRvIII cells, but not in GFP-expressing cells. To identify the Y residues of Dock180 that are phosphorylated by EGFRvIII, we generated Flag-tagged WT and six different Dock180 mutants that lack DHR-1, -2, or other regions (Fig. 2*B*). When EGFRvIII and WT Dock180 were coexpressed in HEK293T cells, EGFRvIII induced p-Y of WT Dock180, whereas expression of either protein alone did not result in p-Y of Dock180 (Fig. 2*C*). Next, we coexpressed EGFRvIII with WT or the six individual mutants of Dock180 and found a marked reduction of EGFRvIII-induced p-Y of the Dock180 Del-6 mutant but not the Dock180 WT or other Del mutants (Fig. 2*D*, blue arrows), suggesting that the p-Y sites are located between amino acid residues 602 and 805 (Fig. 2*B*). In this region, there are six Y residues: Y700, Y712, Y722, Y736, Y760, and Y780. To identify which Y residue is phosphorylated by EGFRvIII, we individually mutated each of these six Y residues to a phenylalanine (F) in the Dock180 Del-5 mutant. When these six Del-5 YF mutants or the Del-5 mutant were separately coexpressed with EGFRvIII in HEK293T cells, EGFRvIII induced p-Y of all Dock180 mutants except Del-5/F722, suggestive of Y722 as a potential p-Y site by EGFRvIII (Fig. 2*E*). To further validate this finding, we generated an Y722F mutation in the full-length Dock180 protein (Dock180^{Y722F}). Coexpression of EGFRvIII with Dock180^{Y722F} showed a more than 40% reduction in p-Y levels compared with that of Dock180^{WT} (Fig. 2*F*). These data suggest that Y722 is a major p-Y site induced by EGFRvIII, and that there are additional p-Y sites within Dock180 because of EGFRvIII activity to a lesser extent. Next, we compared amino acid sequences surrounding Y722 in Dock180 in various species and the other four members of the Dock family, and found that Y722 and most of its surrounding residues are highly conserved among them (Fig. 2*G*).

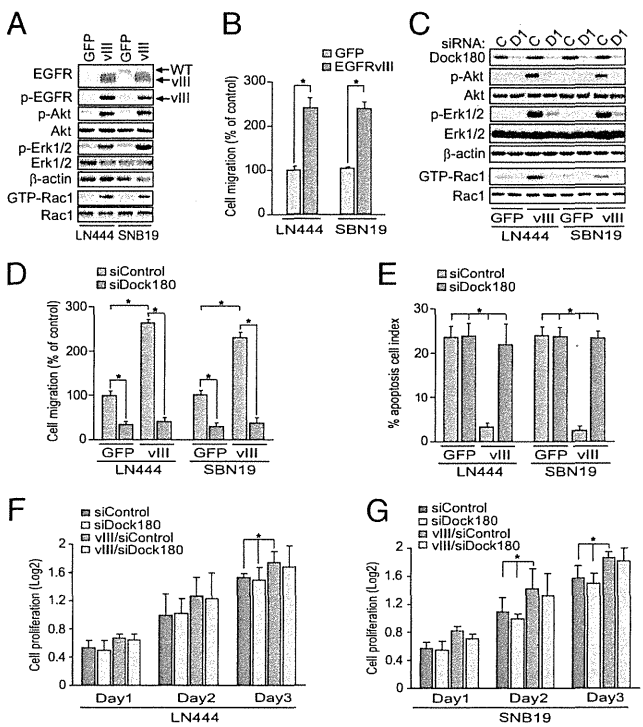

Fig. 1. Dock180 is required for EGFRvIII-induced Rac1 activity, glioblastoma cell migration, and survival in vitro. (*A*) IB analyses. (*B* and *D*) In vitro cell migration assays. Data are presented as percentage of control cells. (*C*) IB analyses. C, control siRNA; D1, Dock180 siRNA pool. In *A* and *C*, β-actin, Akt, Erk1/2, and Rac1 were used as loading controls. (*E*) Cell apoptosis. Data are presented as percentage of apoptotic cells. (*F* and G) Cell proliferation; data were calculated by dividing the total cell number by 50,000 and converting it to a $\log_2$ value. Data in *B* and *D*–*G* were from six replicates per pair per cell line. Data are representative from three independent experiments with similar results. *$P < 0.05$. (Scale bars, ± SD.)

Phosphorylation of Dock180^{Y722} Is Required for EGFRvIII-Promoted Glioblastoma Tumorigenesis. We generated a rabbit polyclonal antibody that specifically recognizes the p-Dock180^{Y722} protein. This anti–p-Dock180^{Y722} antibody detected EGF (but not PDGF or HGF) induced p-Y of endogenous Dock180 in SNB19, U87, U373, and LN444 glioblastoma cells at various levels (Fig. 3*A*). We then knocked down Dock180 in SNB19 or SNB19/EGFRvIII cells using an siRNA pool for Dock180 or a control siRNA (11), and found that depletion of endogenous Dock180 by the siRNA pool, but not control siRNA, significantly diminished the EGFRvIII-induced p-Dock180^{Y722} in SNB19/EGFRvIII cells whereas no signal was seen in SNB19 cells (Fig S2 *A* and *B*). These results validate the specificity of this antibody in detecting EGFRvIII-induced p-Y722 of endogenous Dock180 in glioblastoma cells. Next, we stably transfected Flag-tagged Dock180^{WT} or Dock180^{Y722F} into EGFRvIII-expressing SNB19 and LN444 glioblastoma cells. As shown in Fig. 3*B*, ectopic expression of Dock180^{WT} did not affect EGFRvIII stimulation of p-Akt, p-Erk1/2, and Rac1 activity in SNB19/EGFRvIII and LN444/EGFRvIII cells. In contrast, expression of Dock180^{Y722F} markedly reduced EGFRvIII-induced p-Akt, p-Erk1/2, and Rac1 activity. Additionally, Dock180^{Y722F} but not Dock180^{WT} significantly attenuated EGFRvIII-stimulated glioblastoma cell survival and migration in vitro (Fig. S3 *A* and *B*). However, expression of Dock180^{WT} or Dock180^{Y722F} had only a moderate impact on in vitro proliferation in both LN444/EGFRvIII and SNB19/EGFRvIII cells (Fig. S3 *C* and *D*).

We then separately implanted SNB19/EGFRvIII/Dock180^{WT}, SNB19/EGFRvIII/Dock180^{Y722F}, or the control SNB19/EGFRvIII/GFP cells into the brains of mice. As described previously (12), SNB19/GFP cells formed small but invasive tumors in the brains of mice. Moreover, mice that received SNB19/EGFRvIII/GFP cells showed markedly enhanced tumor growth and invasion, whereas mice that received SNB19/EGFRvIII/Dock180^{WT} cells also developed brain tumors with large volumes and similar invasiveness (Fig. 3*C* and Fig. S4 *A*–*C*), suggesting no further enhancement by Dock180^{WT} expression. In contrast, mice that received SNB19/EGFRvIII/Dock180^{Y722F} cells developed much smaller and less invasive tumors (Fig. 3*C* and Fig. S4 *A*–*C*). In addition, expression of Dock180^{WT} had no significant effect on glioblastoma cell proliferation and survival compared with the controls (Fig. 3 *D* and *E*,

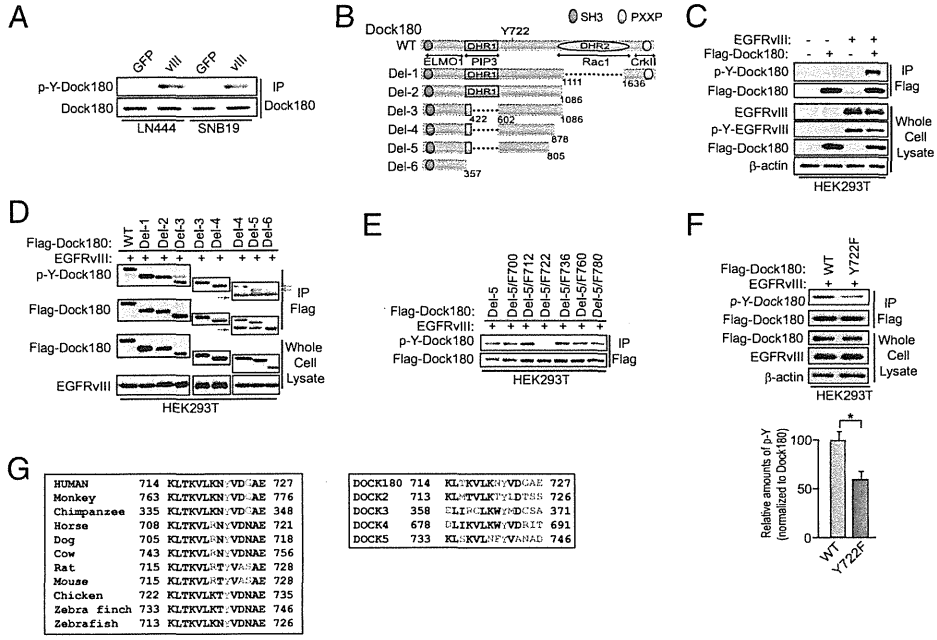

Fig. 2. EGFRvIII induces p-Y of Dock180 at Y722. (*A*) IP and IB analyses. (*B*) Schematic of deletion mutants of Dock180. (*C*) EGFRvIII induces p-Y of Dock180 in HEK293T cells. (*D*) IB analyses. Red arrows, IgG; blue arrows, p-Y of Del mutant. (*E*) Mutation of Y722F in Del-5 decreased p-Y of Dock180. (*F*) Y722 is a major EGFRvIII-induced p-Y site in Dock180. (Scale bars, ± SD.) Bar graph underneath: relative amount of p-Y of Dock180 was determined from three separate in IP-IB blots by ImageJ and normalized to the amount of Dock180. $*P < 0.05$. (*G*) Y722 is conserved in Dock180 of various species and in Dock protein family. Black, conserved amino acids; blue, nonconserved amino acids. In *A* and *C–F*, a pan-phospho-tyrosine antibody was used to detect p-Y-Dock180. Data are representative of three independent experiments with similar results.

and Fig. S4*A*). However, expression of Dock180^{Y722F} significantly suppressed EGFRvIII-stimulated glioblastoma cell proliferation and survival compared with SNB19/EGFRvIII/GFP or SNB19/EGFRvIII/Dock180^{WT} tumors (Fig. 3 *D* and *E* and Fig. S4*A*). These data suggest that p-Dock180^{Y722} is important for EGFRvIII-promoted glioblastoma tumorigenesis in vivo and that Dock180^{Y722F} acts in a dominant negative fashion to inhibit EGFRvIII-driven tumorigenicity.

SFKs Are Responsible for EGFRvIII-Induced p-Dock180^{Y722}. We next performed in silico analyses (http://scansite.mit.edu) and found that Y722 of Dock180 is a potential p-Y site for Src. To determine whether Src and other SFKs are involved in EGFRvIII-stimulated p-Dock180^{Y722} and cell migration, we first treated LN444/EGFRvIII and SNB19/EGFRvIII cells with two pharmacological inhibitors of SFKs (SU6656, PP2) or a vehicle control. As shown in Fig. 4 *A* and *B*, both PP2 and SU6656 effectively inhibited EGFRvIII-induced p-Y of Dock180, Rac1 activity, pan p-Y of Src^{Y418}, and EGFRvIII-stimulated cell migration.

Next, we coexpressed WT, kinase dead (KD) or constitutively activated (CA) Src with flag-tagged Dock180^{WT} or Dock180^{Y722F} in HEK293T cells. WT or CA Src induced p-Y of Dock180^{WT} to higher levels compared with that of Dock180^{Y722F}, whereas KD Src had no effect on p-Y of Dock180^{WT} or Dock180^{Y722F}. As expected, CA Src displayed higher kinase activity on p-Y of Dock180 than did WT Src (Fig. 4*C*). We then tested whether the dominant negative KD Src mutant inhibits the EGFRvIII-induced p-Y of Dock180. As shown in Fig. 4*D*, coexpression of KD

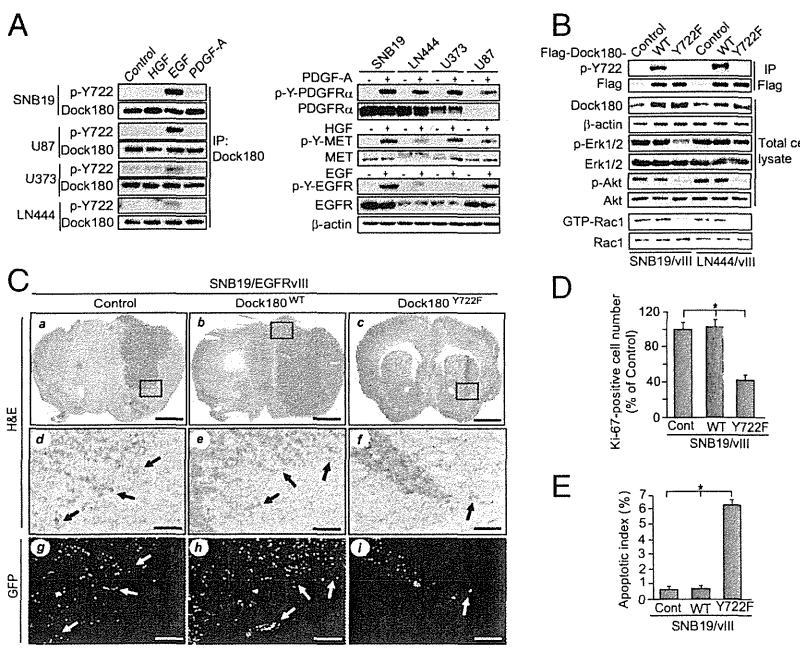

Fig. 3. Phosphorylation of Dock180^{Y722} is critical for EGFRvIII-driven glioblastoma growth and invasion. (*A*) EGF, but not PDGF-A or HGF, induces p-Y of endogenous Dock180^{Y722} (detected with a specific anti–p-Dock180^{Y722} antibody) in glioblastoma cells. (*B*) Effect of Dock180^{WT}, Dock180^{Y722F}, or a vector control on p-Dock180^{Y722}, p-Akt, p-Erk1/2, and Rac1 activity in EGFRvIII-expressing cells. Dock180, Akt, Erk1/2, Rac1, and β-actin were used as loading controls. (*C*) Dock180^{Y722F} inhibits EGFRvIII-promoted glioblastoma growth and invasion in the brain. Representative H&E and IHC images of brain sections of mice receiving various SNB19 cells (8 wk postinjection, five mice per group). (*a–c*) H&E staining. (Scale bars, 1 mm.) (*d–f*) Enlarged areas in *a* to *c* marked with squares. (Scale bars, 200 μm.) (*g–i*) GFP images of the same areas in *d* to *f*. (Scale bars, 200 μm.) Arrows indicate invasive tumor cells (*d–i*). (*D* and *E*) Quantification of Ki-67 and TUNEL staining, respectively. $*P < 0.05$. (Scale bars, ± SD.) Data represent three independent experiments with similar results.

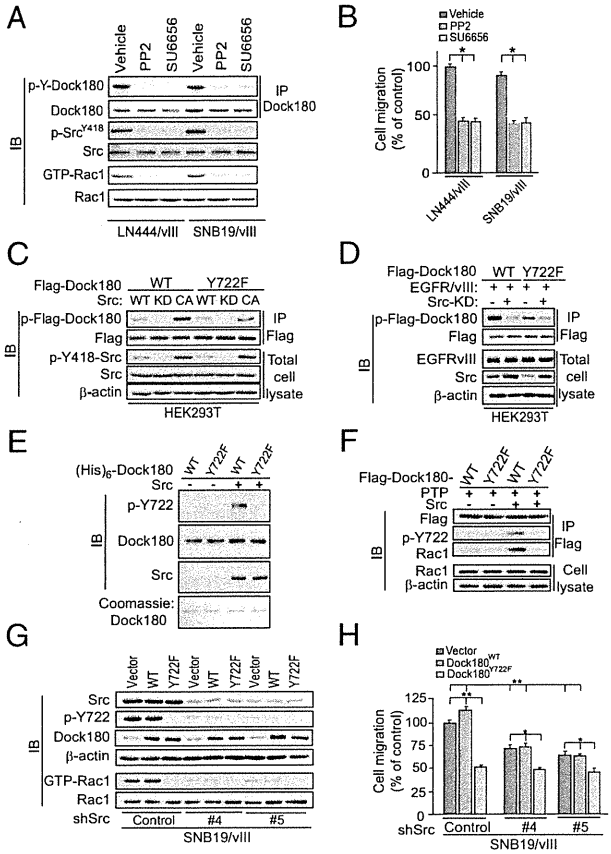

Fig. 4. EGFRvIII-induced p-Dock180^{Y722} is Src-dependent. (*A*) Inhibition of Src by PP2 (2 μM) or SU6656 (2 μM) attenuates EGFRvIII-stimulated p-Y of Dock180 (detected with a pan-phospho-tyrosine antibody, 4G10) and Rac1 activity. (*B*) In vitro cell migration. (*C*) Src phosphorylates Dock180 at Y722 by Src. Dock180^{WT} or Dock180^{Y722F} and WT, a KD or a CA Src were separately coexpressed in HEK293T cells. (*D*) Src-KD inhibits EGFRvIII-induced p-Dock180^{Y722}. (*E*) In vitro Src kinase assay. Various proteins were visualized by Coomassie brilliant blue staining. (*F*) Src-dependent p-Y of Dock180 at Y722 enhances association of Dock180 with Rac1. (*G*) Knockdown of Src inhibits EGFRvIII-induced p-Dock180^{Y722} and Rac1 activation. (*H*) In vitro cell migration. In *A* and *C–G*, Dock180, Src, Rac1, and β-actin were used as loading controls. In *A*, *C*, and *D*, a pan anti–p-Y antibody (4G10) was used to detect p-Y of Dock180. (*E–G*) A specific anti–p-Dock180^{Y722} antibody was used to detect p-Y722 of Dock180. In *B* and *H*, data are presented as percentage of the control from six replicates per pair per cell line. *$P < 0.05$ and **, $P < 0.01$. (Scale bars, ± SD.) Data represent three independent experiments with similar results.

Src with EGFRvIII and Dock180 partially blocked EGFRvIII-induced p-Y of both Dock180^{WT} and Dock180^{Y722F} compared with controls. These results are consistent with partial attenuation of EGFRvIII-induced p-Y by the Dock180^{Y722F} mutant, suggesting that there are other p-Y sites on Dock180 stimulated by EGFRvIII through other kinases.

To validate direct Src phosphorylation of Dock180^{Y722}, we performed in vitro p-Y assays by incubating purified recombinant (His)$_6$-Dock180^{WT} or (His)$_6$-Dock180^{Y722F} proteins with a recombinant active Src followed by immunoblot (IB) using the specific anti–p-Dock180^{Y722} antibody. As shown in Fig. 4*E*, a recombinant Src effectively induced p-Y of Dock180^{WT} but not Dock180^{Y722F} in vitro. Next, we evaluated the impact of Src-induced p-Y of Dock180 on its interaction with Rac1 using an in vitro reconstitution assay. In the absence of the recombinant Src, when immunoprecipitated Dock180^{WT} or Dock180^{Y722F} from HEK293T was dephosphorylated by a protein tyrosine phosphatase, p-Y of Y722 of Dock180 was undetectable and minimal Dock180–Rac1 interaction was observed. However, when a recombinant Src was added, p-Dock180^{WT} but not p-Dock180^{Y722F} was significantly induced, accompanied with an increase in association of Dock180 with Rac1 (Fig. 4*F*).

Then, we stably knocked down endogenous Src using two different shRNAs in SNB19/EGFRvIII cells that expressed either Dock180^{WT} or Dock180^{Y722F}. An ~75% reduction of Src in SNB19/EGFRvIII cells markedly attenuated EGFRvIII-stimulated p-Y722 of Dock180, Rac1 activity (Fig. 4*G*) and cell migration (Fig. 4*H*) in vector control and Dock180^{WT}-expressing cells, but had a minimal impact on Dock180^{Y722F}-expressing cells. Additionally, expression of Dock180^{WT} had minimal impact, whereas Dock180^{Y722F} suppressed EGFRvIII stimulation of p-Dock180^{Y722}, Rac1 activity, and cell migration (Fig. 4 *G* and *H*).

Finally, we determined whether two other SFKs, Fyn and Lyn (13, 14), are involved in EGFRvIII-stimulated Dock180 phosphorylation. We knocked down endogenous Fyn or Lyn using two separate shRNAs for each protein in SNB19/EGFRvIII cells that express Dock180^{WT}, Dock180^{Y722F}, or a vector control. As shown in Fig. 5*A–C*, shRNA knockdown of Fyn or Lyn markedly decreased EGFRvIII-induced p-Y722 of Dock180^{WT}, Rac1 activity, and cell migration in SNB19/EGFRvIII/vector and SNB19/EGFRvIII/Dock180^{WT} cells, but did not affect EGFRvIII stimulation of SNB19/EGFRvIII/Dock180^{Y722F} cells (Fig. 5). These data demonstrate that SFKs, Src, Fyn, and Lyn largely mediate EGFRvIII stimulation of Rac1 activity and glioblastoma cell migration through p-Y722 of Dock180.

SFKs Stimulate p-Dock180^{Y722}, Rac1 Activity, and Cell Migration of Primary Human GBM Cells That Overexpress EGFRvIII. Next, we determined whether SFKs also induce p-Y of Dock180^{Y722}, Rac1 activity, and cell migration in primary human GBM cells. To this end, we examined cells from four different serially transplanted human GBMs, GBM6, GBM39, GBM12, and GBM14 cells that retain the EGFR status of the primary tumor from which they were derived (15). In GBM6 and GBM39 that retained EGFRvIII overexpression, strong p-Y of Dock180^{Y722} and Rac1 activity were found (Fig. S5*A*). In contrast, without EGF stimulation, neither p-Y722 of Dock180 nor increased Rac1 activity was detected in GBM12 cells that express WT EGFR or GBM14 cells that have nondetectable WT EGFR or EGFRvIII. We then treated GBM6 and GBM39 cells with the EGFR inhibitors AG1478 and Erlotinib, the SFK inhibitors SU6656, PP2, its inactive stereoisomer PP3, or vehicle control. These inhibitors markedly attenuated EGFRvIII-induced pan-p-Src^{Y418}, p-Dock180^{Y722}, p-Akt, p-Erk1/2,

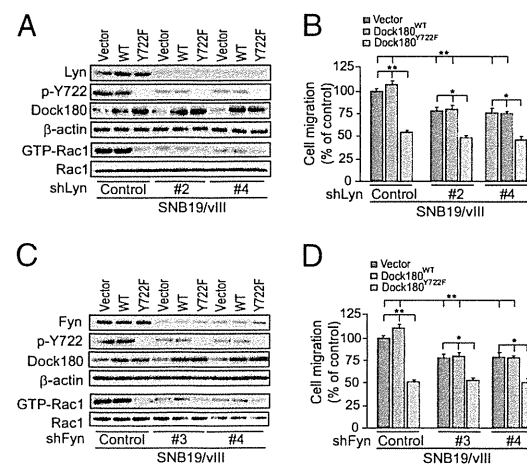

Fig. 5. EGFRvIII-induced p-Dock180^{Y722} is also dependent on SFKs, Fyn and Lyn. (*A* and *C*) Knockdown of Lyn or Fyn inhibits EGFRvIII-induced p-Dock180^{Y722} and Rac1 activation. Dock180, Rac1, and β-actin were used as loading controls. (*B* and *D*) In vitro cell migration assays; data are presented as percentage of the control from six replicates per pair per cell line. *$P < 0.05$ and **, $P < 0.01$. (Scale bars, ± SD.) Data represent three independent experiments with similar results.

Rac1 activity, and cell migration compared with GBM cells treated with PP3 or vehicle control (Fig. S5 *B* and *C*). These results further suggest that SFK-dependent p-Dock180^{Y722} is critical for EGFRvIII-stimulated p-Akt, p-Erk1/2, Rac1 activity, and cell migration in glioblastoma cells.

Coexpression of EGFRvIII, p-Dock180^{Y722} and pan-p-Src^{Y418} in Clinical Glioblastoma Specimens Correlates with an Extremely Poor Prognosis. We performed immunohistochemical (IHC) analysis using antibodies against p-Dock180^{Y722}, EGFRvIII, or p-SrcY^{418} (also detects p-Y of other SFKs) on a cohort of 124 clinical glioblastoma specimens with identifiable central and invasive regions (11). As shown in Table S1, EGFRvIII protein was detected by the specific anti–EGFRvIII-antibody DH8.3 (16) in 36 of 69 GBM (WHO grade IV, 52.2%) and 5 of 26 WHO grade II (19.2%), and 5 of 29 WHO grade III (17.2%) glioblastoma samples, similar to the frequency of EGFRvIII overexpression in clinical GBMs (2). Next, we stained these 46 EGFRvIII-positive tumors and an additional 11 EGFRvIII-negative samples. As shown in Tables S1 and S2, the majority of EGFRvIII-positive tumors demonstrated the presence of p-Dock180^{Y722} and pan-p-Src^{Y418}. Additionally, coexpression of EGFRvIII, p-Dock180^{Y722} and pan-p-Src^{Y418} was found in tumor cells within the invasive areas, as well as in the central regions (Tables S1–S3). An example is shown in Fig. 6*A*, where EGFRvIII was detected in both invasive (Fig. 6*Aa*) and central regions (Fig. 6*Ad*) in a GBM specimen. Interestingly, both pan p-Src^{Y418} and p-Dock180^{Y722} were also expressed in the majority of EGFRvIII-positive tumor cells in invasive and central regions of clinical WHO grade IV and II–III specimens (Fig. 6*A*, *b*, *c*, *e*, and *f*, Fig. S6, and Table S1). In contrast, EGFRvIII, p-Src^{Y418} and p-Dock180^{Y722} were not detected in normal brain tissues. Spearman's rank correlation analysis of expression levels of EGFRvIII and p-Dock180^{Y722} in all of these IHC-stained clinical specimens showed correlation coefficients between border vs. border regions as 0.9000 ($P < 0.05$), center vs. center regions as 0.9747 ($P < 0.05$), and invasive vs. invasive areas as 0.8721 ($P < 0.05$), respectively (Tables S2 and S3).

To further validate these findings, we examined expression of EGFRvIII, p-Src^{Y418}, and p-Dock180^{Y722} in a separate and independent cohort of 38 clinical GBM specimens by IB analyses. As shown in Fig. 6*B*, overexpression of EGFR and EGFRvIII was detected in 10 of 38 (26.3%) GBMs, whereas EGFR was overexpressed in an additional two GBMs, corroborating with the genetic analyses using fluorescent in situ hybridization. Dock180 was expressed at high levels in 25 of 38 GBMs, whereas pan-p-Src^{Y418} was also found in 27 of 38 tumors. Significantly, p-Dock180^{Y722} was coexpressed with pan-p-Src^{Y418} in 7 of 10 EGFR/EGFRvIII-expressing GBMs (tumors 2, 5, 11, 12, 15, 33, and 38), suggestive of the presence of activated EGFR/EGFRvIII-SFK-Dock180-Rac1 signaling in these GBMs. Additionally, Kaplan-Meier analyses showed that in these two independent cohorts, patients with high expression of EGFRvIII or p-Dock180^{Y722} have a shorter overall survival compared with those with low expression of EGFRvIII or p-Dock180^{Y722} (Fig. S7 *A* and *B*). In these cases, a statistically significant correlation was found between worse prognosis of patients with high expression of p-Dock180^{Y722} compared with low expression in the cohort that were analyzed by IHC staining (Fig. S7*A*). When combining the expression status of EGFRvIII and p-Dock180^{Y722} in the analyses, a statistically significant worse prognosis was apparent in glioblastomas with high expression of both proteins compared with those with low expression in both cohorts (Fig. 6*C*). Of note, compared with prognosis of glioblastomas with individual high expression of either EGFRvIII or p-Dock180^{Y722}, the better prognosis value of high expression of both proteins did not appear as drastic as we anticipated. However, this is probably because of the fact that overexpression of EGFRvIII is already a strong prognosis marker for malignant glioblastomas (1, 3) and a relative small number of cases (38 GBM samples) examined by IB analyses. Taken together, these data suggest that p-Dock180^{Y722} could be an independent, as well as an additional, clinically useful marker in the diagnosis and assessment of outcome in GBM with EGFRvIII overexpression.

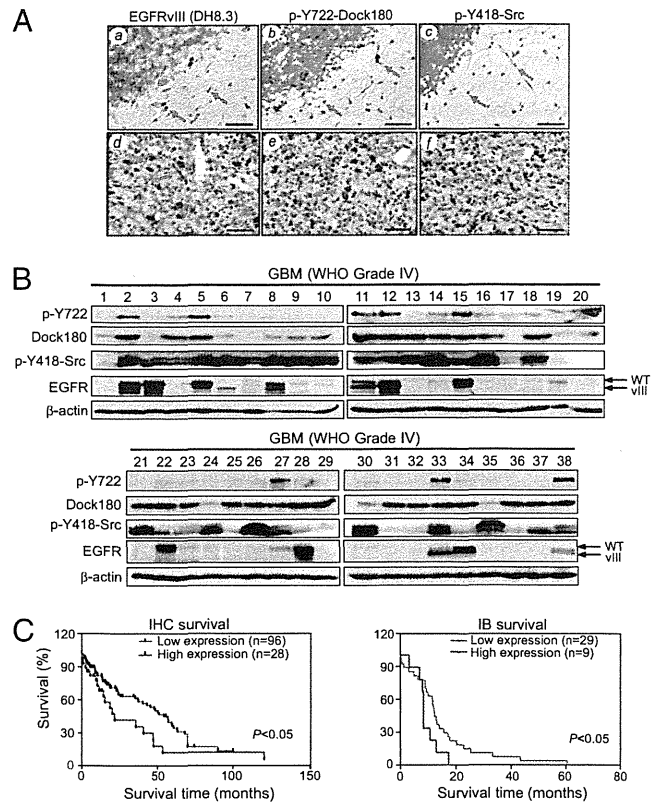

Fig. 6. Coexpression of p-Dock180^{Y722}, EGFRvIII and p-Src^{Y418} correlates with an extremely poor prognosis in patients with glioblastomas. (*A*) IHC analysis. A total of 57 specimens that express EGFRvIII and/or p-Dock180^{Y722} and p-Src^{Y418} are listed in Table S1. Representative images of GBM (grade IV) tissue stained by anti-EGFRvIII (*a* and *d*), anti–p-Src^{Y418} (*b* and *e*), and anti–p-Dock180^{Y722} (*c* and *f*) antibodies. Arrows, positive staining for EGFRvIII, p-Src^{Y418}, and p-Dock180^{Y722}. (Scale bars, 50 μm.) (*B*) IB analysis of a separate and independent cohort of 38 snap-frozen GBM specimens. Dock180 and β-actin were used as loading controls. (*C*) Kaplan-Meier curves with long-rank analyses for patients with high EGFRvIII/p-Dock180^{Y722}–expressing tumors (red line) versus low-expression tumors (blue line) of two separate cohorts of glioblastomas examined in *A* and *B*. *P* values were determined by using the log-rank test. Black bars, censored data. Data represent three independent experiments with similar results.

Discussion

In this study, we report that SFK-dependent p-Dock180^{Y722} mediates downstream EGFRvIII-signaling and glioblastoma growth and invasion. This study highlights four important points. First, Dock180 is required for EGFRvIII-stimulated glioblastoma cell migration and survival in vitro. Second, EGFRvIII induces a specific p-Y of Dock180 at Y722 and mutation of this p-Y site inhibits EGFRvIII-promoted glioblastoma cell migration and survival in vitro and tumor growth and invasion in vivo. Third, SFKs, Src, Fyn, and Lyn mediate EGFRvIII induction of phosphorylation of Dock180^{Y722} in glioblastoma cells stimulating tumorigenesis. Fourth, p-Dock180^{Y722} and p-Src^{Y418} are coexpressed with EGFRvIII in clinical glioblastoma specimens. Coexpression of EGFRvIII, p-Dock180^{Y722} and p-Src^{Y418} is correlated with an extremely poor prognosis in patients with glioblastomas. Taken together, our results suggest that SFK activation of p-Dock180^{Y722}-Rac1 signaling plays a critical role in EGFRvIII-driven glioblastoma tumorigenesis.

GEFs couple RTKs to Rac1 (9) and Dock180 is a downstream effector of EGFR-mediated cell migration in *Drosophila* (10). Here, we show that EGFRvIII induces SFKs-dependent p-Dock^{Y722}, thereby activating Rac1-signaling and promoting glioblastoma cell growth, survival, and invasion. Rac1 is downstream

of Dock180 (8) and modulates cell growth, survival, and motility (17). Consistent with this finding, inhibition of Dock180 by siRNA knockdown, overexpression of a Dock180^{Y722F} mutant, or suppression of SFKs impaired EGFRvIII-stimulated Rac1 activity and tumorigenesis. Moreover, EGFRvIII also activates the PI3K-Akt and MAPK pathways (3, 4) and induces a cytokine circuit that stimulates EGFR-signaling in neighboring tumor cells (18). Separate disruption of these downstream pathways inhibits EGFRvIII function, underscoring the heterogeneity of clinical glioblastomas. This heterogeneity is also illustrated by the fact that activated p-Src^{Y418} is detected in all 38 clinical glioblastoma samples, whereas EGFRvIII and p-Dock180^{Y722} are only expressed in 8 of 38 specimens. Similarly, in a total of 124 clinical glioblastoma specimens analyzed by IHC, p-Dock180^{Y722} and p-Src^{Y418} were not detected in a number of tumors that express EGFRvIII, suggesting that other signaling pathways are also involved in EGFRvIII-driven tumorigenesis. The heterogeneity of glioblastomas involved p-Y of Dock180 is further demonstrated by our recent study, showing that a Src-dependent p-Y of Dock180 mediates PDGFRα, another RTK that is often overexpressed in proneural subtype of human glioblasotmas (1–3), and promoted glioblastoma tumorigenesis. Moreover, PDGFRα/Src-induced p-Y of Dock180 is at another tyrosine residue of Dock180 (19), indicating a distinct signaling from PDGFRα/Src. Taken together, our results show that SFK-dependent p-Y of Dock180 mediates EGFRvIII and PDGFRα stimulation of Rac1 signaling, cell growth, survival, and invasion in glioblastomas.

Src, Lyn, and Fyn are expressed in clinical glioblastoma samples and EGFRvIII-expressing glioblastoma cells. Inhibition of Src, Lyn, or Fyn attenuated EGFRvIII-promoted tumorigenesis and invasion (13, 14). Our data are consistent with and extend these findings. We found that Src directly induces phosphorylation of Dock180^{Y722} and interaction of Dock180 with Rac1 in vitro and in glioblastoma cells. Moreover, inhibition of Src, Lyn, and Fyn by pharmacological inhibitors or shRNA knockdown reduces EGFRvIII-induced p-Dock180^{Y722}, Rac1 signaling and migration of glioblastoma cells. Coexpression of p-Dock180^{Y722}, EGFR, and EGFRvIII and p-Src^{Y418} in clinical glioblastoma tumor specimens correlates with an extremely poor prognosis. Therefore, our results integrate SFK-activated p-Dock180^{Y722}-Rac1 signaling in EGFRvIII-driven tumorigenesis.

It has been postulated that nonstimulated Dock180 assumes an inhibitory configuration in which the SH3 domain folds back and interacts with DHR-2 domain, preventing access of Rac1. Upon ELMO1 binding, folded Dock180 is opened to allow Rac1 binding to the DHR-2 domain (8). Similarly, the N terminus of a Rho GEF Vav1 interacts with its Dbl homology (DH) domain, thereby inhibiting GTPase binding (7). Moreover, a Src-induced p-Y of Vav1 at its N terminus opens the DH domain for Rac1 binding (7). Our data are consistent with this mechanism. We show that SFK-dependent p-Dock180^{Y722} is required for Dock180 activation of Rac1, thereby mediating EGFRvIII-promoted tumorigenesis. However, Y722 is not located in the identified functional domains but at the boundary of a helix/coil configuration in the DHR-1/DHR-2 interdomain of Dock180 (20). With the helix/coil repeats of the interdomain, the DHR-1 domain is brought into close apposition with DHR-2 and Rac1, bringing the membrane binding elements of DHR-1 and Rac1 into the same coplanarity, thereby enabling simultaneous membrane association of the ELMO1-Dock180-Rac1 complex. Additionally, a Dock180-Rac1 dimer is formed that binds to the membrane (20). Therefore, SFK-induced p-Y722 could be critical for the interdomain of Dock180 that holds DHR-1 adjacent to DHR-2 to form a dimeric complex and to achieve the activation of Rac1.

In summary, our data connect the sustained activation of EGFRvIII and SFKs to the p-Dock180^{Y722} that stimulates Rac1 signaling and malignant behavior of human glioblastoma cells. This unique link is underscored by coexpression of EGFRvIII, p-Src^{Y418} and p-Dock180^{Y722} in clinical glioblastoma specimens and association with extremely poor prognoses. Because activation of EGFRvIII and SFKs renders an aggressive glioblastoma phenotype and the induced p-Y of Rho GEF is a common mechanism that activates Rac1 signaling, our results suggest that targeting the EGFRvIII-SFK-Dock180-Rac1 pathway could offer hope in treating malignant glioblastomas with EGFRvIII overexpression.

Materials and Methods

For descriptions of cell lines, cell cultures, reagents, antibodies, DNA constructs, IB and IP, purification of recombinant proteins, in vitro Src tyrosine phosphorylation, pull-down assays of the binding of Dock180 with Rac1, and statistical analysis, see *SI Materials and Methods*. Experiments using animals were performed using a protocol that was reviewed and approved by the University of Pittsburgh Institutional Animal Care and Use Committee. Studies using human tissues were reviewed and approved by the Institutional Review Board involving Human Subjects at the University of Pittsburgh, Pittsburgh, PA.

ACKNOWLEDGMENTS. We thank M. Matsuda, S. Courtneidge, R. Pieper, E. van Meir, and Y. Zhou for providing reagents. This work was supported by National Institutes of Health Grants CA130966 (to S.-Y.C.) and CA102583 (to K.V.); a grant from the James S. McDonnell Foundation (to B.H.); a grant from the Pennsylvania Department of Health, and Innovative Research Scholar Awards (to S.-Y.C. and B.H.); Mayo Specialized Program of Research Excellence Grants CA108961 (to J.N.S.), CA106429 (to C.K.T.), and CA95616 (to W.K.C., and F.B.F.); Grant HL070561 and the National Basic Research Program of China Grant 2011CB964801 (to T.C.); an award from the Goldhirsh Foundation (to F.B.F.); and a Clinical Fellowship from the Victorian Cancer Center (to T.G.J.). W.K.C. is a fellow of the National Foundation for Cancer Research. This project used the shared facilities at the University of Pittsburgh Cancer Institute that were supported in part by National Institutes of Health Grant P30CA047904.

1. Van Meir EG, et al. (2010) Exciting new advances in neuro-oncology: The avenue to a cure for malignant glioma. *CA Cancer J Clin* 60:166–193.
2. Cancer Genome Atlas Research Network (2008) Comprehensive genomic characterization defines human glioblastoma genes and core pathways. *Nature* 455: 1061–1068.
3. Furnari FB, et al. (2007) Malignant astrocytic glioma: Genetics, biology, and paths to treatment. *Genes Dev* 21:2683–2710.
4. Huang PH, Xu AM, White FM (2009) Oncogenic EGFR signaling networks in glioma. *Sci Signal* 2:re6.
5. Nishikawa R, et al. (1994) A mutant epidermal growth factor receptor common in human glioma confers enhanced tumorigenicity. *Proc Natl Acad Sci USA* 91: 7727–7731.
6. Cai XM, et al. (2005) Protein phosphatase activity of PTEN inhibited the invasion of glioma cells with epidermal growth factor receptor mutation type III expression. *Int J Cancer* 117:905–912.
7. Rossman KL, Der CJ, Sondek J (2005) GEF means go: Turning on RHO GTPases with guanine nucleotide-exchange factors. *Nat Rev Mol Cell Biol* 6:167–180.
8. Côté JF, Vuori K (2007) GEF what? Dock180 and related proteins help Rac to polarize cells in new ways. *Trends Cell Biol* 17:383–393.
9. Schiller MR (2006) Coupling receptor tyrosine kinases to Rho GTPases—GEFs what's the link. *Cell Signal* 18:1834–1843.
10. Duchek P, Somogyi K, Jékely G, Beccari S, Rørth P (2001) Guidance of cell migration by the *Drosophila* PDGF/VEGF receptor. *Cell* 107:17–26.
11. Jarzynka MJ, et al. (2007) ELMO1 and Dock180, a bipartite Rac1 guanine nucleotide exchange factor, promote human glioma cell invasion. *Cancer Res* 67:7203–7211.
12. Hu B, et al. (2009) ADP-ribosylation factor 6 regulates glioma cell invasion through the IQ-domain GTPase-activating protein 1-Rac1-mediated pathway. *Cancer Res* 69:794–801.
13. Stettner MR, et al. (2005) Lyn kinase activity is the predominant cellular Src kinase activity in glioblastoma tumor cells. *Cancer Res* 65:5535–5543.
14. Lu KV, et al. (2009) Fyn and Src are effectors of oncogenic epidermal growth factor receptor signaling in glioblastoma patients. *Cancer Res* 69:6889–6898.
15. Giannini C, et al. (2005) Patient tumor EGFR and PDGFRA gene amplifications retained in an invasive intracranial xenograft model of glioblastoma multiforme. *Neuro-oncol* 7:164–176.
16. Jungbluth AA, et al. (2003) A monoclonal antibody recognizing human cancers with amplification/overexpression of the human epidermal growth factor receptor. *Proc Natl Acad Sci USA* 100:639–644.
17. Burridge K, Wennerberg K (2004) Rho and Rac take center stage. *Cell* 116:167–179.
18. Inda MM, et al. (2010) Tumor heterogeneity is an active process maintained by a mutant EGFR-induced cytokine circuit in glioblastoma. *Genes Dev* 24:1731–1745.
19. Feng H, et al. (2011) Activation of Rac1 by Src-dependent phosphorylation of Dock180Y1811 mediates PDGFRα-stimulated glioma tumorigenesis in mice and humans. *J Clin Invest* 121:4670–4684.
20. Premkumar L, et al. (2010) Structural basis of membrane targeting by the Dock180 family of Rho family guanine exchange factors (Rho-GEFs). *J Biol Chem* 285: 13211–13222.

J Neurosurg 119:1331–1339, 2013

Cadherin 13 overexpression as an important factor related to the absence of tumor fluorescence in 5-aminolevulinic acid–guided resection of glioma

Laboratory investigation

Tomonari Suzuki, M.D.,[1] Satoru Wada, Ph.D.,[2,4] Hidetaka Eguchi, Ph.D.,[2,3] Jun-ichi Adachi, M.D., Ph.D.,[1] Kazuhiko Mishima, M.D., Ph.D.,[1] Masao Matsutani, M.D., Ph.D.,[1] Ryo Nishikawa, M.D., Ph.D.,[1] and Masahiko Nishiyama, M.D., Ph.D.[2,3,5]

[1]Department of Neuro-Oncology/Neurosurgery, International Medical Center, Hidaka; [2]Project Division and [3]Division of Translational Research, Research Center for Genomic Medicine, Saitama Medical University, Hidaka; [4]Information Technology Center, Saitama Medical University, Moroyama; and [5]Department of Molecular Pharmacology and Oncology, Gunma University Graduate School of Medicine, Maebashi, Japan

Object. Gliomas contain aggressive malignant cancer, and resection rate remains an important factor in treatment. Currently, fluorescence-guided resection using orally administered 5-aminolevulinic acid (5-ALA) has proved to be beneficial in improving the prognosis of patients with gliomas. 5-ALA is metabolized to protoporphyrin IX (PpIX) that accumulates selectively in the tumor and exhibits strong fluorescence upon excitation, but glioma cells do not always respond to 5-ALA, which can result in incomplete or excessive resection. Several possible mechanisms for this phenomenon have been suggested, but they remain poorly understood. To clarify the probable mechanisms underlying the variable induction of fluorescence and to improve fluorescence-guided surgery, the authors searched for key negative regulators of fluorescent signal induced by 5-ALA.

Methods. A comprehensive gene expression analysis was performed using microarrays in 11 pairs of tumor specimens, fluorescence-positive and fluorescence-negative tumors, and screened genes overexpressed specifically in fluorescence-negative tumors as the possible candidates for key negative regulators of 5-ALA–induced fluorescence. The most possible candidate was selected through annotation analysis in combination with a comparison of expression levels, and the relevance of expression of the selected gene to 5-ALA–induced fluorescence in tumor tissues was confirmed in the quantified expression levels. The biological significance of an identified gene in PpIX accumulation and 5-ALA–induced fluorescence was evaluated by in vitro PpIX fluorescence intensity analysis and in vitro PpIX fluorescence molecular imaging in 4 human glioblastoma cell lines (A1207, NMCG1, U251, and U373). Knockdown analyses using a specific small interfering RNA in U251 cells was also performed to determine the mechanisms of action and genes working as partners in the 5-ALA metabolic pathway.

Results. The authors chose 251 probes that showed remarkably high expression only in fluorescent-negative tumors (median intensity of expression signal > 1.0), and eventually the cadherin 13 gene *(CDH13)* was selected as the most possible determinant of 5-ALA–induced fluorescent signal in gliomas. The mean expression level of *CDH13* in the fluorescence-negative gliomas was statistically higher than that in positive ones ($p = 0.027$), and knockdown of *CDH13* expression enhanced the fluorescence image and increased the amount of PpIX 13-fold over controls ($p < 0.001$) in U251 glioma cells treated with 5-ALA. Comprehensive gene expression analysis of the *CDH13*-knockdown U251 cells demonstrated another two genes possibly involved in the PpIX biosynthesis: ATP-binding cassette transporter *(ABCG2)* significantly decreased in the *CDH13* knockdown, while oligopeptide transporter 1 *(PEPT1)* increased.

Conclusions. The cadherin 13 gene might play a role in the PpIX accumulation pathway and act as a negative regulator of 5-ALA–induced fluorescence in glioma cells. Although further studies to clarify the mechanisms of action in the 5-ALA metabolic pathway would be indispensable, the results of this study might lead to a novel fluorescent marker able to overcome the obstacles of existing fluorescence-guided resection and improve the limited resection rate.
(http://thejns.org/doi/abs/10.3171/2013.7.JNS122340)

Key Words • **5-aminolevulinic acid** • **glioma** • **cadherin 13** • **photodynamic diagnosis**

Abbreviations used in this paper: ABC = ATP-binding cassette; *ACTB* = actin, beta; ALAD = aminolevulinate dehydratase; ALAS = aminolevulinate synthase; ATP = adenosine 5′-triphosphate; CDH13 = cadherin 13; CPOX = coproporphyrinogen oxidase; DMEM = Dulbecco modified Eagle medium; *FECH* = ferrochelatase; GAPDH = glyceraldehyde 3-phosphate dehydrogenase; HMBS = hydroxymethylbilane synthase; PEPT1 = peptide transporter 1; PpIX = protoporphyrin IX; PPOX = protoporphyrinogen oxidase; RT-PCR = reverse transcription polymerase chain reaction; SAM = significance analysis of microarrays; siRNA = small interfering RNA; UROD = uroporphyrinogen decarboxylase; UROS = uroporphyrinogen III synthase; 5-ALA = 5-aminolevulinic acid.

Gliomas contain aggressive, malignant forms of cancer.[9,14] Despite improvement in chemoradiotherapy, high-grade glioma is often fatal. The effect of current standard therapy using temozolomide with radiation for glioblastoma, the most malignant type of glioma, is marginal, and the median survival time is merely 1.3 years.[29]

Surgery continues to be the mainstay treatment for gliomas. The resection rate is a key determinant of prognosis,[13,24] with the most difficult obstacle being the unclear tumor margin during resection. To remove tumor

without damaging the normal adjacent tissues, Stummer et al. first attempted photodynamic diagnostic surgery using 5-aminolevulinic acid (5-ALA) in 1998 and demonstrated that normal brain tissue revealed no porphyrin fluorescence, whereas tumor tissue was distinguished by bright red fluorescence due to the response of glioma to 5-ALA.[28] Currently, fluorescence-guided resection is widely applied,[18,20,25,33] and it has certainly improved the resection rate and prognosis for gliomas. A randomized, controlled, Phase III trial demonstrated that the overall resection rate (65% vs 36%, respectively) and 6-month progression-free survival rate (41% vs 21%, respectively) were significantly improved in the 5-ALA assigned group compared with the control group.[27] Nevertheless, it is now widely recognized that glioma cells do not always respond to 5-ALA even in the same patient, and the heterogeneous response can cause an incomplete or excessive resection in some cases. Several possible mechanisms for this phenomenon have been suggested, but they remain poorly understood.[4,7,30,32]

5-ALA is metabolized to the protoporphyrinogen IX in mitochondria via the heme biosynthesis pathway and is finally converted to protoporphyrin IX (PpIX) by a protoporphyrinogen IX oxidase. The synthesized PpIX densely accumulates in the tumor cells and shows bright fluorescence upon excitation with blue light. Various transporters, or factors, have been suggested to be involved in the PpIX biosynthesis pathways, including ferrochelatase *(FECH)* in tumor cells.[32] None of these factors alone, however, has proved consistently critical in the mechanisms of PpIX accumulation,[11] so more important mechanisms and key regulators might exist in the PpIX biosynthesis pathways and the induction mechanism of fluorescence by 5-ALA.

In this study, we attempted to select possible determinants of the fluorescent signal induced by 5-ALA using comprehensive gene expression analysis to clarify the probable mechanisms underlying the variable induction of fluorescence.

Methods

Cell Lines

Four human glioblastoma cell lines (A1207, NMCG1, U251, and U373) were used in this study. The U251 cells were obtained from American Type Culture Collection; A1207 and U373 were kindly donated by Dr. Webster K. Cavenee of the Ludwig Institute for Cancer Research; and NMCG1 was kindly provided by Dr. T. Todo at the University of Tokyo. All tumor cells were cultured in Dulbecco modified Eagle medium (DMEM) containing 10% fetal bovine serum and maintained at 37°C in air containing 5% CO_2.

Clinical Samples

A total of 70 patients with diagnosed brain tumors were enrolled in this study between March 2006 and January 2009. Among these 70 patients, 16 with gliomas were eligible for the study according to the study criteria, which were patients with a tumor containing both positive and negative fluorescence signal sites induced by 5-ALA. Of the 16 gliomas, 11 were diagnosed as glioblastomas, and histopathological diagnoses of the other 5 gliomas were anaplastic astrocytoma, anaplastic ependymoma, anaplastic oligodendrogliomas, oligoastrocytoma, and pilocytic astrocytoma. Patients were orally administered 20 mg/kg of 5-ALA (Cosmo Bio) 4 hours before the operation, and fluorescence was determined using a semiconductor laser with a VLD-M1 spectrometer (M&M Co., Ltd.) at surgery. Based on the fluorescent signals, we collected tissue samples from each patient at surgery (both fluorescence-positive and fluorescence-negative tumor sites). All samples were immediately frozen and stored at −80°C until microarray and real-time reverse transcription polymerase chain reaction (RT-PCR) analyses. The study was approved by the Ethics Committee at Saitama Medical University, and written informed consent was obtained from all patients.

RNA Isolation and Quality Determination

Total RNA was extracted from frozen tissue samples and glioblastoma cells using the RNA Nucleospin RNAII kit (Macherey-Nagel) according to the manufacturer's protocols. The quality of total RNA was determined with a 2100 Bioanalyzer (Agilent Technologies) to check the RNA integrity number; we chose samples with an RNA integrity number greater than 7.0.

DNA Microarray Analysis

Comprehensive gene expression analysis was performed using the Agilent Whole Human Genome Oligo Microarray Kit (4 × 44K; Agilent Technologies) as previously reported.[22] The scanned image data were analyzed with Agilent Feature Extraction software (version 9.5, Agilent Technologies), and gene expression signals were normalized using GeneSpring GX (Agilent Technologies) and further analyzed using Spotfire software (Tibco Software).

Statistical Methods to Select Candidate Genes

Initially, the analytical probes were determined according to 2 criteria: the probes had an observed expression intensity greater than 0 in over half of the samples and had a coefficient variation value greater than 0.3. Among the analytical probes, the candidates, which were differently expressed between 5-ALA–induced fluorescence-positive and fluorescence-negative samples, were selected. To do so, we referred to the fold-change values in the expression intensity and further used the significance analysis of microarrays (SAM) statistical method.[34] In the SAM method, the differences were ranked, and a small positive constant was added to the denominator of the gene-specific t-test to omit genes with low expression values. Multiple comparison of PpIX fluorescence intensity was conducted using 1-way ANOVA, followed by the Dunnett test, using U373 cells as the referent. Statistical calculations were performed using "R" statistical software (http://www.r-project.org/) with the "samr" package.[34] Ingenuity Pathways Analysis (Ingenuity Systems) was used in screening candidate genes for 5-ALA–induced PpIX accumulation- and cancer-related factors.[15]